Catena 207 (2021) 105600

Contents lists available at ScienceDirect

Catena

journal homepage: www.elsevier.com/locate/catena

Hydrological, geomorphic and sedimentological responses of an alpine basin to a severe weather event (Vaia storm)

R. Rainato [a,*], L. Martini [a], G. Pellegrini [a], L. Picco [a,b,c]

[a] Department of Land, Environment, Agriculture and Forestry, University of Padova, Padova, Italy
[b] Universidad Austral de Chile, Faculty of Engineering, Valdivia, Chile
[c] Universidad Austral de Chile, RINA – Natural and Anthropogenic Risks Research Center, Valdivia, Chile

ARTICLE INFO

Keywords:
Vaia storm
Mountain basin
Large flood
Geomorphic changes
Sediment transport
Boulder mobility

ABSTRACT

To achieve a reliable analysis of the impacts induced in mountain basins by large and infrequent floods, all their main components, from the spatial-temporal distribution of meteorological agents to the hydrological, geomorphic and sedimentological response should be considered. Comprehensive study of the hydro-geomorphic responses is extremely valuable to increase the awareness of large floods, especially, in highly populated mountain areas. Such type of investigation requires a solid and wide dataset, which is why only few studies had the chance to describe the response in such a holistic way. This work comprehensively analyzed the high magnitude/low frequency Vaia event, a severe storm that affected northeastern Italy in October 2018 and thus the Rio Cordon study basin. The 80 h precipitation registered in the basin showed a total rainfall equal to 29.8% of the mean annual precipitation. The temporal distribution of rainfall presented two phases, i.e., a first characterized by moderate but persistent precipitation and a second more intense, exhibiting recurrence intervals over 50 years. A combination of indirect methods permitted the reconstruction of the hydraulic forcing acted in the Rio Cordon. Despite the implicit uncertainty, these methods clearly highlighted the high magnitude expressed by October 2018 flood, which generated a unit peak discharge equal to 3.3 $m^3 s^{-1} km^{-2}$ and a peak of unit stream power of 3865 W m^{-2}, i.e., the highest hydraulic forcing conditions ever observed in 34 years. In terms of geomorphic changes, the use of pre- and post-event LiDAR data stressed out a moderate response of the hillslopes, where the (re)activation of the sediment sources was limited. Only few of these acted as sediment supplier to the main channel. The channel network instead, exhibited an evident response, with the Rio Cordon severely altered by wide lateral widening, deep streambed incision and armouring removal. The hydraulic and geomorphic forcing generated by October 2018 flood caused extensive streambed remobilization and boulder mobility that, in turn, induced the transport of a massive sediment volume. In this sense, the match between bedload observed and bedload predicted suggested the outstanding hydraulic forcing occurred and the quasi-unlimited supply conditions acted during the flood. The long-lasting monitoring program maintained in the Rio Cordon basin provided the rare opportunity to compare two high magnitude/low frequency floods and their induced effects. The September 1994 and October 2018 events were caused by different rainfall conditions, which resulted in different hydrological- and, especially, geomorphic- and sedimentological-responses. Particularly, the October 2018 flood induced an unprecedented alteration on the fluvial system, the effects of which could persist over the long-term.

1. Introduction

Large and infrequent floods are hydrological events characterized by high magnitude and low frequency occurrence, which can impact mountain basins and their fluvial systems over large temporal and spatial scales. In alpine environments, these flood events can be induced by intense summer thunderstorms (Shakti et al., 2017), prolonged rainfalls (Brogan et al., 2019), rapid snowmelt (Friele et al., 2020), rain-on-snow event (Pomeroy et al., 2016) and sudden water release from glacier sources (Bohorquez and Darby, 2008). All these triggering factors converge in a main effect that is the generation of massive runoff characterized by high water discharges and stream power peaks. An

* Corresponding author.
E-mail address: riccardo.rainato@unipd.it (R. Rainato).

https://doi.org/10.1016/j.catena.2021.105600
Received 18 February 2021; Received in revised form 5 July 2021; Accepted 10 July 2021
Available online 20 July 2021

extensive literature found these conditions associated to flash floods, i.e., rapid and severe floods (McEwen and Werritty, 1988; Batalla et al., 1999; Borga et al., 2014; Marchi et al., 2016; Lucía et al., 2018), whereas they were observed less frequently in large floods of long duration (Cassandro et al., 2002; Sholtes et al., 2018; Bucała-Hrabia et al., 2020). The characterization of the hydraulic forcing conditions expressed by high magnitude/low frequency events can be challenging, with the frequent need to rely on indirect methods as post-flood measurements, dendrogeomorphic analysis, paleoflood estimation and hydraulic modelling in order to reconstruct hydrographs and peak discharges (Rico et al., 2001; Stoffel and Bollschweiler, 2008; Victoriano et al., 2018; Wyzga et al., 2020). In this sense, a delineation of large and infrequent events based on peak of water discharge or unit peak discharge appears not fully defined, with values spanning over several orders of magnitude (Marchi et al., 2016; Amponsah et al., 2018), while a minimum threshold of 300 W m^{-2} was reported in terms of unit stream power (Miller, 1990; Magilligan, 1992). However, it is worth noting that this threshold was based on geomorphic effectiveness of floods and that mountain basins responses are highly variable. Indeed, the geomorphic response to a high magnitude/low frequency flood can include: (i) the formation of rockfalls (Heckmann and Schwanghart, 2013), debris flows (Pastorello et al., 2020) and landslides (Korup, 2005) along the hillslopes; (ii) bedforms alteration (Lenzi, 2001), channel narrowing (Liébault and Piégay, 2002), chute cutting and channel migration (Gorczyca et al., 2013), reach straightening (Bauch and Hickin, 2011), lateral widening with floodplain erosion (Wicherski et al., 2017) or increase in channel bars extent (Hajdukiewicz et al., 2016) along the fluvial system. The investigation of these geomorphic changes is traditionally accomplished by multi-temporal geomorphological mapping, using both field and remote sensing products, such Digital Elevation Models (DEMs) and aerial photos (Messenzehl et al., 2014; Carrivick et al., 2016; Vericat et al., 2017). Additionally, geomorphic variations in mountain streams are quantified using the widely known DEM of Difference (hereinafter DoD) technique, which can be also used to infer in-channel sediment transfer's efficiency (Lane et al., 2003; Vericat et al., 2014; Cucchiaro et al., 2019; Calle et al., 2020). In mountain basins, the hydraulic forcing and geomorphic changes generated by high magnitude/low frequency floods can intensify the ordinary sediment transfer processes, altering the sediment cascade from source areas to the fluvial system (Brierley et al., 2006; Burt and Allison, 2010; Fryirs, 2013). However, during and after a large infrequent event, the capability of a catchment to promote or impede the sediment cascade depends on the impact of such event on the degree of (dis)connectivity. Specifically, highly connected catchments react transmitting a sediment pulse throughout the system, whereas in disconnected catchments the pulse is stopped by landform impediments (Fryirs et al., 2007). Along the fluvial system, the sediment dynamics promoted by high magnitude/low frequency floods can stretch over various time scales. Typical effects induced at event scale are streambed remobilization (Piton and Recking, 2017), boulder mobility (Turowski et al., 2009; Gob et al., 2010), high transport rates (D'Agostino and Lenzi, 1999; Pagano et al., 2019) and massive transported volumes (Rickenmann, 1997; Baewert and Morche, 2014). Nonetheless, the induced effects can also act on longer time scales, augmenting the transport rate of subsequent floods and favoring a memory effect on the sediment dynamics (Rainato et al., 2017; Uchida et al., 2018; Rickenmann, 2020; Korup, 2005).

High magnitude/low frequency floods caused by severe weather events were poorly investigated and rarely analyzed from the rainfall-runoff conditions to geomorphic and sedimentological effects. A recent example of severe weather event was the Vaia storm, which affected the Northeast Italy on October 27–30, 2018. This storm generated extremely high wind gusts, storm surges and heavy precipitation that caused landslides, floods, interruption of electric supply, road traffic disruption and the worst forest loss ever documented in Italy, consisting of about 8.5 million m^3 of growing stock felled over 41,000 ha (Biolchi et al., 2019; Cavaleri et al., 2019). This work aims at defining the responses of an alpine basin to the Vaia storm, focusing on: (i) the determination of rainfall and hydraulic forcing conditions, (ii) the analysis of the geomorphic and sedimentological responses showed by hillslopes and main channel, (iii) the comparison of these responses with those exhibited by the alpine basin over the last three decades.

2. Material and methods

2.1. Study area

2.1.1. Study basin

The Rio Cordon basin (Fig. 1) is a mountain basin extending for 5 km^2 in the eastern Italian Alps (Dolomites). It is characterized by typical alpine climatic conditions with a mean annual precipitation of 1180 mm (1986–2018). The runoff regime can be defined as nivo-pluvial due to the predominance of snowfalls between November-April, while short rain showers and persistent precipitations prevail in summer and autumn, respectively. The basin is part of the Southern Limestone Alps with the geological substrate mainly composed by dolomites, limestones, volcanic conglomerates (Wengen group) and calcareous-marly rocks (Buchenstein group). A rugged topography can be appreciated throughout the basin, which exhibits an average slope of 27°. Due to the basin elevation between 1763 and 2763 m a.s.l., spruce and larch forest covers merely 7% of catchment area, while bare rock (14%), shrubs (18%) and grassland (61%) are more widespread. In the basin, the third-order Rio Cordon stream flows on a rough channel bed, featuring boulder-cascade and step-pool morphologies (*sensu* Montgomery and Buffington, 1997). In 2014, the surface streambed material resulted poorly sorted with $D_{16}/D_{50}/D_{84}/D_{90}$ of grain size distribution (GSD) equal to 29/114/358/455 mm, respectively, and a well-developed armour layer (Rainato et al., 2018a). The main channel (hereinafter Rio Cordon) had an average slope of 17% with a mean bankfull width equal to 5.3 m and a bankfull discharge (Q_{Bf}) = 2.30 m^3 s^{-1} (Lenzi et al., 2006a; Mao and Lenzi, 2007). Along the basin, the Rio Cordon is interrupted by a waterfall, which represents a topographic knickpoint

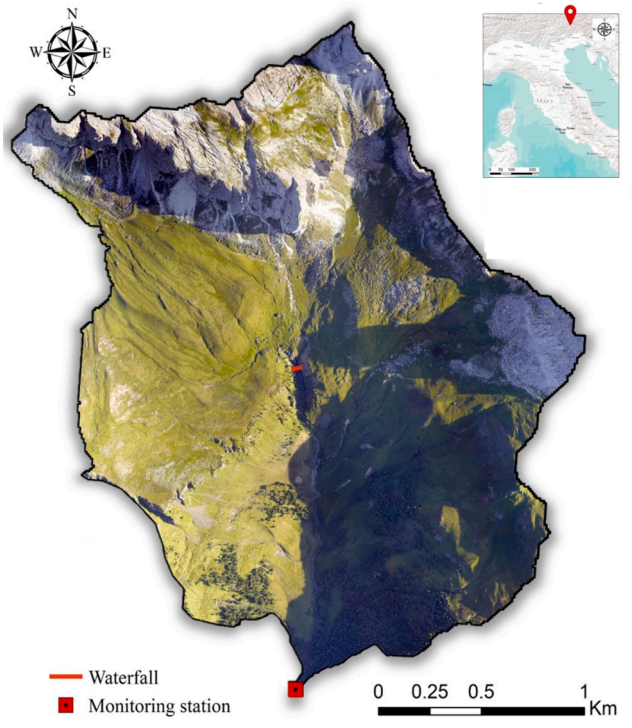

Fig. 1. The Rio Cordon basin, located in the eastern Italian Alps. The waterfall represents the topographic knickpoint that divides the upper part (upper plateau) and lower part of the basin.

that conventionally divides the whole basin into the upper part (upper plateau) and lower part (Rainato et al., 2018b). In 2016, 420 sediment source areas were detected throughout the basin, classified in debris flow channel/deposit, erosional area, stream bank erosion, landslide, rockfall deposit and active talus (Ferrato et al., 2017). From the sources, the sediment can be transported downstream and eventually deposited at the outlet (1763 m a.s.l.), where a permanent monitoring station is built.

2.1.2. Long-lasting monitoring program

In 1985, the Rio Cordon basin was instrumented thanks to a collaboration between University of Padova and Veneto Region, and operating since 1986 under the ARPA Veneto management (Regional Department for Land Safety). Specifically, a permanent monitoring station was set up at the basin outlet with the aim of continuously monitor water discharge (Q), suspended sediment load (SSL) and bedload (BL). In 1994, the monitoring station was provided with a meteorological station, which measure continuously air temperature, wind speed and precipitations through a heated rain gauge. Between September 1986 and September 2018, the monitoring station recorded 33 flood events (Supplementary S1). Overall, these events mobilized 1850 m^3 of coarse material, corresponding to a bedload yield of 3154 t. Considering instead the total sediment yield ($BL + SSL$), the Rio Cordon basin delivered ~15125 t. Among the 33 events recorded, the highest magnitude was expressed by the September 1994 flood, when an intense summer shower triggered a flash flood with a peak of water discharge (Q_P) equal to 10.40 $m^3\ s^{-1}$ (Rainato et al., 2017). This event altered the basin by modifying the streambed configuration, creating new sediment sources throughout the catchment and causing the transport of about 900 m^3 of coarse material, which corresponds to ~50% of the total bedload volume observed between September 1986 and September 2018.

2.2. Rainfalls

Consistently to the previous flood event investigations realized in the Rio Cordon basin (Lenzi and Marchi, 2000; Rainato et al., 2018a; Oss Cazzador et al., 2020), to describe the rainfalls induced by the Vaia storm the data from the heated rain gauge were used. This sensor measures every 5 min with an accuracy of 0.2 mm, permitting to determine the total precipitation and the rainfall intensities exhibited by the storm event. Specifically, the maximum rainfall intensities in 5, 15, 30 min and 1, 3, 6, 12, 24, 48, 72 h were determined and named, I_{5min}, I_{15min}, I_{30min} and I_{1h}, I_{3h}, I_{6h}, I_{12h}, I_{24h}, I_{48h}, I_{72h}, respectively. To better comprehend the magnitude expressed by Vaia storm in the Rio Cordon basin, the measured rainfall intensities were compared to the rainfall depth-duration-frequency (DDF) curves compiled by ARPA Veneto for the "Passo Falzarego" meteorological station. This was chosen as the nearest rain gauge with a long-lasting monitoring. In fact, it is located 9.4 km north-west of the Rio Cordon basin, at 2040 m a.s.l., and operates since 1985.

2.3. Hydrological conditions

The wind and rainfall generated by the Vaia storm caused the arrest of the water level gauges installed in the Rio Cordon monitoring station. Therefore, no discharge measurement was realized during the Vaia induced flood event (hereinafter October 2018 event). In light of this, to describe the hydraulic forcing conditions that acted in the Rio Cordon, indirect methods were used. To reconstruct the hydrograph, the nearest gauging station operating during the Vaia storm was tested. This was the "Sottorovei" Arpa Veneto gauging station (5.2 km south-west of the Rio Cordon basin), which recorded the discharge of the Fiorentina Stream (Q_{Fi}). Worth noting is that the Rio Cordon is a sub-basin of the Fiorentina basin (58 km^2). To test the capacity of Fiorentina discharge (Q_{Fi}) to describe the Rio Cordon discharge (Q_{Rc}), two recent floods (November 2012 and November 2014) recorded in the sub-basin were isolated and the measured Q_{Rc} were compared to the Q_{Fi} simultaneously recorded. Using linear regression and comparing 1762 discharge measurements, it was possible to observe that Q_{Fi} and Q_{Rc} were statistically correlated ($R^2 = 0.897$, p-value < 0.01). Therefore, the Q_{Fi} measured during the Vaia storm were scaled according to the linear equation obtained, permitting to reconstruct the hydrograph of the October 2018 flood in the Rio Cordon. However, it should be stressed that this reconstruction was affected by a certain degree of uncertainty as based on the analysis of near-bankfull events. In fact, in terms of Q_P, the November 2012 and November 2014 floods ranged between 2.06 and 2.10 $m^3\ s^{-1}$ in the Rio Cordon, while in the Fiorentina Stream spanned between 23.60 and 32.00 $m^3\ s^{-1}$. Therefore, given the high magnitude expressed by October 2018 flood, a specific investigation about Q_P was made in order to integrate the hydrograph reconstructed with a portion devoted to describing the peaking part. The latter was intended as the hydrograph part simulated between the maximum discharges estimated by hydrograph reconstruction ($Q_{Fi} - Q_{Rc}$ relationship) and the Q_P estimated. A simple triangular shape was used to describe this peaking part, according to the hydrograph shapes generated in mountain basins by high magnitude/low frequency floods (Lenzi et al., 1999; Turowski et al., 2009).

The value of Q_P was calculated through two different approaches. Firstly, post-event surveys permitted to clearly identify high-water marks along a cross section located in the final straight reach of Rio Cordon and embanked on the right side, i.e., the best conditions for Q_P definition by the slope conveyance method (Gaume and Borga, 2008; Marchi et al., 2016). A differential Global Position System (dGPS) device, featuring an average vertical and horizontal accuracy <0.05 m, was used to survey this cross section, which was used to compute Q_P through the Manning-Strickler equation (Eq. (1)):

$$Q = \frac{AR^{\frac{2}{3}}S^{\frac{1}{2}}}{n} \quad (1)$$

in which Q is the water discharge ($m^3\ s^{-1}$), A the flow area (m^2), R the hydraulic radius (m), S the stream slope (m m^{-1}) and n the Manning roughness coefficient. Based on field observation of the boundary roughness conditions and on the n observed in mountain streams (Reid and Hickin, 2008; Zink and Jennings, 2014, Oss Cazzador et al., 2021) a Manning roughness coefficient = 0.125 $s^{-1}\ m^{-1/3}$ was applied.

Secondly, the equation (Eq. (2)) proposed by Bravard and Petit (1997) to determine Q_P through a basin area scaling ratio was used:

$$q = Q(a/A)^c \quad (2)$$

in which q is the water discharge occurred in a sub-basin (in $m^3\ s^{-1}$), Q the water discharge measured at the basin outlet (in $m^3\ s^{-1}$), a is the sub-basin area (in km^2), A the basin area (in km^2), while c is a site specific coefficient that in literature varies between 0.4 and 1.0 (Gob et al., 2010). The maximum Q_{Fi} recorded during the Vaia storm were used as Q, while c equal to 0.8 was applied according to Liébault et al. (2012) and Oss Cazzador et al. (2021).

Once determined the hydrograph and its peaks, the bedload duration (T_{Bl}) and the effective runoff (ER) were estimated. These describe the hydrograph-duration and -volume exceeding the threshold for bedload motion. To this end, the critical discharge (Q_C) for motion of coarse streambed material observed in the Rio Cordon during the period 2012–2018 was used, which corresponds to $Q_C = 2.06\ m^3\ s^{-1}$ (Rainato et al., 2020). This is consistent with the observations made in the Rio Cordon by Lenzi et al. (1999), who documented Q_C constantly around $Q = 2.00\ m^3\ s^{-1}$ in the flood events of 1987–1994.

The hydraulic forcing conditions were expressed even in terms of unit stream power (ω), through Eq. (3):

$$\omega = \frac{\rho g Q S}{w} \quad (3)$$

where ρ is the fluid density (kg m^{-3}), g the acceleration due to gravity (m s^{-2}), Q the water discharge (m^3 s^{-1}), S the stream slope (m m^{-1}) and w is the flow width (m). Specifically, to calculate the peak of unit stream power (ω_P) acted during the October 2018 flood, the flow width was determined by analyzing the Digital Terrain Model (DTM) of the Rio Cordon dated 2006 (see Section 2.4), which suggested a $w = 6.30$ m.

2.4. Geomorphic setting

2.4.1. Remote sensing data

To investigate the geomorphic response induced in the Rio Cordon basin by the Vaia storm, two LiDAR surveys dated, respectively, 2006 and 2019 were exploited. Both surveys produced classified point clouds and orthophotos. The latter with resolution of 0.5 m and 0.2 m, for 2006 and 2019, respectively. From the point clouds, only the ground points were used to derive the DTMs for the following analyses. The post-processing was carried out using CloudCompare software (www.danielgm.net/cc; version 2.10.2 Zephyrus), with the primary aim of co-registering the point clouds. The co-registration was performed using a combination of automatic Iterative Closest Point (ICP) algorithm and manual definition of point correspondences. The compound use of these methods wants to provide a suitable solution to reduce unrealistic differences between the point clouds that often exist in rugged environments (Cucchiaro et al., 2020). The orthophotos were exploited for different purposes: from the qualitative assessment of the changes throughout the basin to the analysis of the variations along active channel and sediment source areas. However, due to the time interval between the two LiDAR surveys, other events might have contributed to alter the geomorphic setting of the catchment. To distinguish the alterations induced by these events from the October 2018 effects, an additional pre-event orthophoto and previous studies were used. Specifically, the 2015 orthophoto (Web Map Service service for AGEA, 0.20 m resolution) and the geomorphic effects documented in Rainato et al. (2017, 2018a) and Oss Cazzador et al. (2020) were taken advantage of. Instead, the two DTMs permitted to determine the topographic differences and, then, any significant geomorphic change related to the Vaia storm.

2.4.2. Geomorphic change detection

The topographic differences were determined by comparative analysis between the 2006 and 2019 DTMs, using the DEM of Difference, hereinafter DoD, technique. The old-2006 DTM was subtracted to the new-2019 DTM using the Geomorphic Change Detection 7.4.4, AddIn for ArcGIS (Wheaton et al., 2010). To overcome the mere representation of all the changes, hence to distinguish those changes produced by noise from the real ones, a widely used approach accounting for spatially distributed elevation uncertainty was adopted. Also, this approach overcomes spatially uniform methods, i.e. minimum level of detection (minLOD), in which real geomorphic changes risk to be removed. The methodology proposed by Wheaton et al. (2010) mainly regards three steps to generate a robust DoD output: (i) computation of cell-by-cell DEM uncertainty (spatial distribution of elevation uncertainty) using the Fuzzy Inference System (FIS); (ii) propagation of the uncertainty into the DoD; (iii) statistical significance of the propagated uncertainty based on probabilistic thresholding. The first step was accomplished using a three inputs-FIS, i.e., point density, slope and roughness. Particularly, the roughness information was derived using the Roughness Index, proposed by Cavalli and Marchi (2008), and already applied in other geomorphological studies as part of the three inputs-FIS (Oss Cazzador et al., 2021). The second step regards the propagation of the uncertainty from the individual DEM into the DoD, still on cell by cell basis. This step was accomplished by applying the well-known combined error formula proposed by Brasington et al. (2000). The third step assessed the statistical significance of the DoD output using a 95% probabilistic thresholding, which means that all the elevation changes that do not fit within a confidence interval of 95% were discarded. The application of such probabilistic thresholding relies upon the choice of the corresponding t-value, as proposed by Taylor (1997) and then by Brasington et al. (2003) and Lane et al. (2003). In this work, a conservative 95% confidence interval (t-value = 1.96) was assigned because of the high values of elevation uncertainty and the willingness to quantify the minimum compatible volume of sediment mobilized in the Rio Cordon basin. The DoD was performed to investigate sediment displacement occurred along the hillslope, within the lower Rio Cordon and at the bedload storage area of the monitoring station. Specifically, for the hillslopes, the aim was to outline potential new sediment sources that may or not have contributed to supply sediment in the channel network. At the bedload storage area, the DoD was performed over a polygon of 4200 m^2, which includes also the lateral and downstream zones buried by sediment. However, an area of ~500 m^2 was affected by the presence of a bridge that passes over the deposit. Here, no suitable LiDAR data were found so that the 2006 and 2019 DTMs have been roughly interpolated causing an estimated source of error of about 11%.

2.4.3. Sediment sources

The detection of the new sediment sources was accomplished through orthophotos and DoD interpretation with a focus to the lower part of the basin. In addition, a previous sediment source inventory (Ferrato et al., 2017), was used to help the detection of those areas (re) activated only during the Vaia storm. The sediment sources were then grouped according to the classification already proposed for the Rio Cordon basin in: landslide, debris flow channel/deposit, surficial erosion, stream bank erosion, rockfall and active talus. Knowing the coupling state of the sediment sources, it is possible to have an idea of the volume of sediment supplied to the channel network and eventually to the outlet. To assess the coupling state and the potential supply from sources to active channel, an approach based on the Index of Connectivity (IC) (Cavalli et al., 2013) and the DoD was proposed. First, using the 2019 orthophoto, the sources that did not reach the active channel and, therefore, visibly decoupled were excluded. Then, the IC map was computed with SedInConnect 2.3 (Crema and Cavalli, 2018), using the pre-event (2006) DTM, selecting the active channel as target. The mean IC value for each sediment source was extracted and only those having a value higher than a threshold were considered. The threshold was set as the median (50th percentile) of all the mean IC values of each area. In other terms, a boundary based on the central value was set, to distinguish areas of high- and low-IC. Finally, the sediment sources showing predominant erosion (negative net volume difference) were selected. In this way, we assumed that only the sediment sources highly coupled with the active channel supplied a significant volume of sediment. Conversely, the decoupled or balanced (erosion and deposition balanced) sediment sources were not considered suppliers. In particular cases, e.g. landslides recharging debris flow channels/deposits, the balance was obtained as the overall DoD result of the single areas composing the same potential supplier.

2.4.4. Active channel

The active channel variations were first investigated through qualitative analysis of orthophotos. To further investigate the geomorphic changes as well as its causes and effects along the Rio Cordon, the active channel was segmented into sub-reaches. The segmentation, which draws part of the criteria from Rinaldi et al. (2013), considered homogeneous sub-reaches based on stream slope, channel width and confluences with tributaries. Stream slope was derived from the 2006 DTM, while channel width and confluences from the orthophotos. Hence, six sub-reaches (1–6) ranging from 154 m to 623 m in length were identified in the lower basin, resulting in 2023 m totally investigated along the active channel. Upper Rio Cordon was excluded from this analysis due to its semi-colluvial nature and sediment disconnectivity documented during Vaia storm (Oss Cazzador et al., 2021). The width ratio (Wr), the peak of unit stream power (ω_{Pi}) acted during the October 2018 event and

the DoD segregation (Wheaton et al., 2013) were calculated for each sub-reach. *Wr* is intended as the ratio between the post- and pre-flood average channel width (Scorpio et al., 2018), which were assessed on the 2019 and 2006 orthophotos, respectively. The peak of unit stream power occurred in the sub-reaches ($\omega_{P1} - \omega_{P6}$) was determined according to Eq. (3). To this end, each *S* and *w* were calculated analyzing the 2006 DTM and considering the stream slope and the channel width averaged on the upstream channel portion. Instead, the maximum water discharge flowed in each sub-reach (i.e. *Q* in Eq. (3)) was determined using the Eq. (2), with *Q* equal to the Q_P calculated for the Rio Cordon outlet (see Section 2.3), while *a* and *A* were the basin area subtended by the sub-reach and the whole basin, respectively. Finally, the potential correlations between *Wr*, ω_{Pi} and DoD were investigated through linear regression.

2.5. Sedimentological setting

The sedimentological response of the study basin to the Vaia storm was explored by investigating the variation in the grain size distribution of the main channel and by characterizing and quantifying the coarse material transported. To determine the post-flood GSD of the Rio Cordon, 202 particles were collected and measured along the main channel using the grid by number method. The same method was used to describe the GSD of bedload transported to the monitoring station, which was estimated by sampling 224 particles. Also, the ten largest boulders deposited at the bedload storage area were characterized in terms of *a*-, *b*- and *c*-axis in order to describe the boulder mobility triggered by the October 2018 flood. To determine the volume of coarse material mobilized by the event (BL_{Obs}), the bedload storage area of the monitoring station was surveyed. Therefore, using the DoD technique (see Section 2.4.2) it was possible to quantify a reliable volume resulting from the elevation difference between the post-event storage unit (2019 DTM) and the pre-event one (2006 DTM). The reconstruction of hydraulic forcing conditions occurred during the October 2018 event enabled the volume of coarse material transported to be predicted (BL_{Pred}) as well. To this end, consistently with previous Rio Cordon flood investigations (D'Agostino and Lenzi, 1999; Lenzi et al., 1999, 2006b; Rainato et al., 2017), the bedload equation (Eq. (4)) proposed by Schoklitsch (1962) was used:

$$Q_S = \frac{2.5}{\rho_s/\rho} S^{\frac{3}{2}} (Q - Qc) \quad (4)$$

where Q_S is the bedload rate ($m^3\ s^{-1}$) and ρ_s is the sediment density (kg m^{-3}), respectively. The use of Schoklitsch equation permitted to calculate BL_{Pred} but also to analyze its performance under the different hydrological conditions examined in the Rio Cordon over the last decades.

3. Results

3.1. Rainfall characterization

In the Rio Cordon basin, the Vaia storm induced a rainfall event that lasted about 80 h, starting on October 27th at 06:55 (CET) and ending on October 30th at 14:45 (Table 1). During this time interval, a total precipitation of 352.0 mm was recorded, corresponding to the 29.8% of the mean annual precipitation. The rainfall event was not continuous but exhibited a hiatus of ~9 h (Fig. 2). Therefore, it is possible to identify a first and a second phase, hereinafter Phase 1 and Phase 2. The Phase 1 lasted 36.8 h with 199.8 mm, while 152.0 mm were recorded in the 34.2 h of Phase 2.

The event registered a mean rainfall intensity equal to 4.4 mm h^{-1}, while Phase 1 and Phase 2 expressed an average of 5.4 and 4.4 mm h^{-1}, respectively (Table 1). Phase 1 showed a higher mean intensity due to the more continuous precipitation over time compared to Phase 2 that exhibited an abrupt decrease after peaking (Fig. 2). However, the highest intensities between I_{5min} and I_{12h} were constantly observed during Phase 2, particularly, between 8:30 and 21:30 of October 29th. In this sense, the maximum rainfall intensities recorded ($I_{5min} - I_{72h}$) were compared to the DDF curves of the "Passo Falzarego" meteorological station. Fig. 2b and 2c show that I_{5min}, I_{15min} and I_{30min} resulted lower than DDF curve estimated for recurrence interval (*RI*) of 2 years, while from I_{1h} progressively exceeded the DDF curves by culminating in $I_{6h} - I_{72h}$ that showed *RI* clearly higher than 50 years.

Table 1
Main characteristics of the first and second phase of the rainfall event recorded by the Rio Cordon rain gauge during the Vaia storm, as well as of the entire rainfall event. I_{5min}, I_{15min}, I_{30min} describe the maximum rainfall intensities measured in 5, 15 and 30 min, respectively. I_{1h}, I_{3h}, I_{6h}, I_{12h}, I_{24h}, I_{48h} and I_{72h} are the maximum intensities recorded, respectively, in 1, 3, 6, 12, 24, 48 and 72 h.

	Phase 1	Phase 2	Event
Time of rainfall initiation (CET)	27/10/2018 06:55	29/10/2018 04:30	27/10/2018 06:55
Time of rainfall end (CET)	28/10/2018 19:45	30/10/2018 14:45	30/10/2018 14:45
Total precipitation duration (h)	36.8	34.2	79.8
Total precipitation (mm)	199.8	152.0	352.0
Mean rainfall intensity (mm h^{-1})	5.4	4.4	4.4
Time of I_{5min} (CET)	28/10/2018 07:15	29/10/2018 19:05	29/10/2018 19:05
I_{5min} (mm/5 min)	2.2	4.2	4.2
I_{15min} (mm/15 min)	5.6	7.0	7.0
I_{30min} (mm/30 min)	9.2	12.4	12.4
I_{1h} (mm/1h)	14.6	20.4	20.4
I_{3h} (mm/3h)	34.8	42.0	42.0
I_{6h} (mm/6h)	74.4	85.2	85.2
I_{12h} (mm/12 h)	111.2	111.8	111.8
I_{24h} (mm/24 h)	176.6	142.8	176.6
I_{48h} (mm/48 h)	–	–	295.0
I_{72h} (mm/72 h)	–	–	343.2

3.2. Hydraulic forcing conditions

The reconstructed hydrograph estimated *Q* persistently >1.10 $m^3\ s^{-1}$ (i.e. >0.5 Q_{Bf}) from October 28th at 7:00 through October 31st at 9:30. Two consecutive peaks were determined, respectively, on October 28th at 18:45 and on October 29th at 20:00, interspersed by ~21 h of under-bankfull conditions (Fig. 3). Therefore, similarly to what observed in the rainfall analysis, also in the flood event caused in the Rio Cordon by the Vaia storm two phases can be observed (Fig. 3).

The reconstructed hydrograph suggested Q_P for the Phase 1 and Phase 2 equal to 2.31 $m^3\ s^{-1}$ and 8.24 $m^3\ s^{-1}$, respectively. Interestingly, the maximum discharge exhibited a delay respect to the maximum I_{5min} of 55 min (Table 2). The high-water marks detected in the post-flood surveys enabled to calculate, via Eq. (1), a maximum peak flowed = 17.50 $m^3\ s^{-1}$. Such peak was related to the maximum discharge occurred, i.e., Q_P of Phase 2. No field evidences permitted to determine the Q_P of Phase 1. For both phases, the peak of water discharge was estimated through the basin area scaling ratio (Eq. (2)) applied to the maximum *Q* recorded in the Fiorentina Stream. Thus, the Q_P estimated were 3.43 $m^3\ s^{-1}$ and 15.21 $m^3\ s^{-1}$ for Phase 1 and Phase 2, respectively (Table 2). These peaks resulted roughly consistent to those estimated for the Phase 1 by the hydrograph reconstruction (lower by a factor of 0.67) and for the Phase 2 by the post-flood surveys (higher by a factor of 1.15). Therefore, considering the uncertainty and limits associated to each method used, the average between Q_P estimated by hydrograph reconstruction (2.31 $m^3\ s^{-1}$) and the one determined by basin area scaling ratio (3.43 $m^3\ s^{-1}$) was considered representative in describing the water discharge peak of Phase 1. About Phase 2, the average between Q_P obtained by post-flood surveys (17.50 $m^3\ s^{-1}$) and the one resulted by application of basin area scaling ratio (15.21 $m^3\ s^{-1}$) was considered.

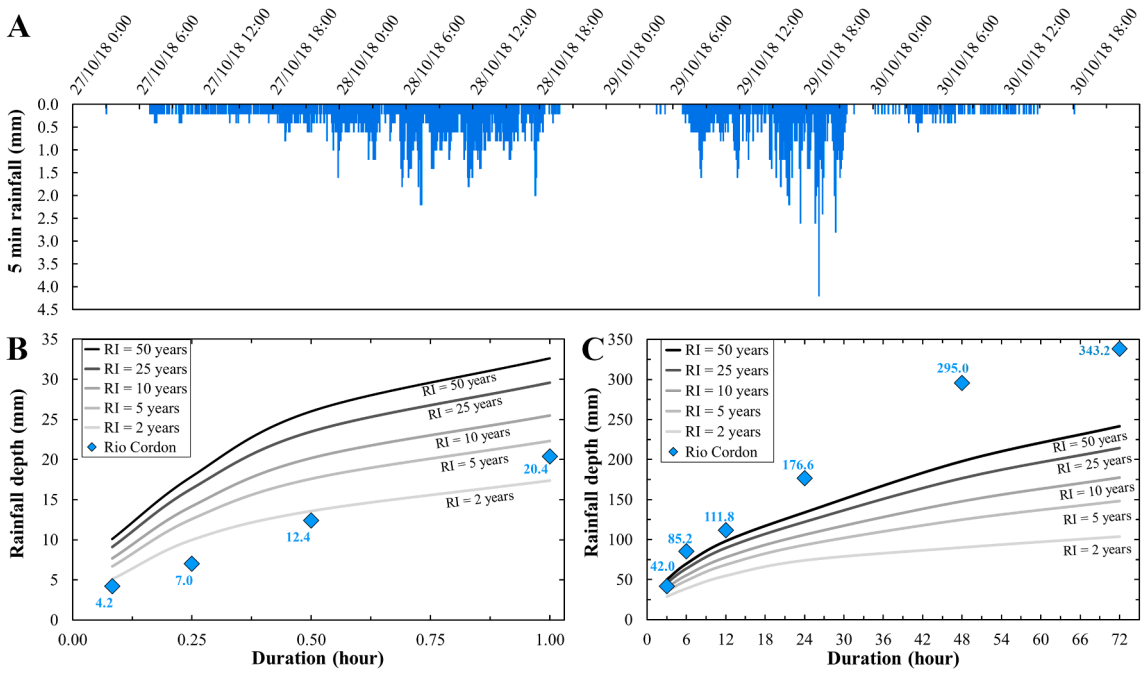

Fig. 2. (A) Rainfall recorded by Rio Cordon meteorological station during Vaia storm; (B) Maximum rainfall intensities recorded in 5 (I_{5min}), 15 (I_{15min}), 30 (I_{30min}), 60 (I_{1h}) minutes and (C) in 3 (I_{3h}), 6 (I_{6h}), 12 (I_{12h}), 24 (I_{24h}), 48 (I_{48h}) and 72 (I_{72h}) hours compared to the rainfall depth-duration-frequency curves of Passo Falzarego rain guage.

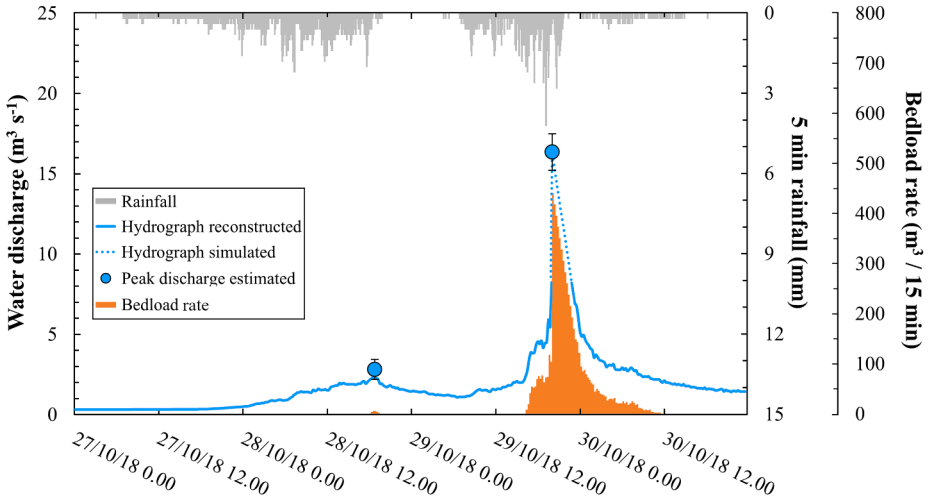

Fig. 3. Rainfall, water and bedload discharges estimated for the October 2018 event. The blue line represents the hydrograph reconstructed starting from the Fiorentina discharge measurements; the blue dotted line are the parts of hydrograph simulated between the maximum values estimated by discharge reconstruction ($Q_{Fi} - Q_{Rc}$ relationship) and the peaks discharge estimated for the first and second phase of flood event. The peaks discharge are represented by the blue circles, the error bars are the lower and upper bounds of the Q_P considered. The orange lines express the bedload rate calculated by the Schoklitsch (1962) equation.

Hence, Phase 1 and Phase 2 expressed $Q_P = 2.87$ (± 0.56) m^3 s^{-1} and $Q_P = 16.36$ (± 1.14) m^3 s^{-1}, respectively (Fig. 3). In terms of unit stream power, these peaks corresponded to 678 W m^{-2} and 3865 W m^{-2}. The resulted hydrograph shows a Phase 1 characterized by a lower magnitude compared to Phase 2. In terms of flow duration, in Phase 1 about 0.50 h with $Q > Q_{Bf}$ and 1.75 h of bedload duration (T_{Bl}) were assessed. Such conditions led to an effective runoff (ER) equal to 1.0×10^3 m^3 (Table 2). Phase 2 exhibited a clear higher magnitude: over-bankfull discharge for ~18 h was observed and Q two- and three-fold higher than Q_{Bf} were noted for 5.75 h and 3.50 h, respectively. In Phase 2, $ER = 200 \times 10^3$ m^3 and T_{Bl} equal to 20.25 h were estimated, leading the total bedload duration for the October 2018 flood to 22 h (Table 2). Overall, the October 2018 flood expressed the largest Q_P (16.36 m^3 s^{-1}) and ER (201×10^3 m^3) ever documented in the Rio Cordon basin, with a unit peak discharge equal to 3.3 m^3 s^{-1} km^{-2}.

3.3. Geomorphic effects

3.3.1. Sediment source areas and sediment connectivity

The detection of the sediment sources led to the mapping of 9 newly formed instabilities and 17 source areas reactivated or enlarged during the October 2018 flood (Fig. 4A). The new sediment sources were exclusively located in the lower part of the Rio Cordon basin, covering a total area of 31,179 m^2, with a minimum extent of 49 m^2 and a maximum of 4927 m^2. According to the sediment sources' classification used in the Rio Cordon basin, 5 sources were classified as debris flow channels/deposits, 20 as landslides and 1 as stream bank erosion.

The sediment connectivity analysis pointed out the presence of 6 sources coupled to the channel network and potentially sediment suppliers (Fig. 4A). Conversely, 20 sources were classified as non-supplier, either because decoupled to the active channel or because they did not show net erosion. This result agrees with the historic knowledge of the

Table 2
Main characteristics of first and second phase of the flood event induced in the Rio Cordon by Vaia storm, and of the entire flood. Q_{Bf} indicates the Rio Cordon bankfull discharge (i.e., 2.30 $m^3 s^{-1}$), while Q_{2Bf} and Q_{3Bf} represent discharges, respectively, two and three fold larger. T_{Bl} is the estimated bedload duration, while *ER* is effective runoff. BL_{Pred} and BL_{Obs} describe the bedload volume calculated by applying the Schoklitsch (1962) equation and by DoD analysis, respectively.

	Phase 1	Phase 2	Event
Duration of $Q > Q_{Bf}$ (h)	0.50	17.75	18.25
Duration of $Q > Q_{2Bf}$ (h)	–	5.75	5.75
Duration of $Q > Q_{3Bf}$ (h)	–	3.50	3.50
T_{Bl} (h)	1.75	20.25	22.00
ER (10^3 m^3)	1.0	200.0	201.0
Time of Q_P (CET)	28/10/2018 18:45	29/10/2018 20:00	29/10/2018 20:00
Q_P (hydrograph reconstructed[a]; $m^3 s^{-1}$)	2.31	8.24	8.24
Q_P (post-flood survey; $m^3 s^{-1}$)	–	17.50	17.50
Q_P (basin area scaling ratio[b]; $m^3 s^{-1}$)	3.43	15.21	15.21
BL_{Pred} (m^3)	32	6858	6890
BL_{Obs} (m^3)	–	6656	6656

[a] Hydrograph reconstruction based on the Fiorentina discharge measurements.
[b] Based on Bravard and Petit (1997) equation.

basin and with post-event observations. The estimated volume of sediment eroded from the 6 coupled sources was 1219 m^3, mostly conveyed by the landslides-debris flow system located close to the outlet (Fig. 4A). This volume was reduced, subtracting the bedload yields expressed by November 2012 and June 2014 events (Supplementary S1) to avoid double counting, thus obtaining a potential volume supplied during the October 2018 flood of 1140 m^3.

3.3.2. Active channel

Between pre- and post-event conditions, over the 2023 m analyzed, the active channel widened from an average width of 6.30 m to 10.60 m, expanding from 8607 m^2 to 38696 m^2. Considering the geomorphic change detection, the DoD analysis computed a total net erosion of 6979 m^3 ± 2059 m^3 unevenly distributed along the reach (Fig. 4A). The average depth of surface lowering (erosion) was 1.06 m, while the average depth of surface raising (deposition) was 0.63 m. Many of the deeper erosional areas were located along the banks (Fig. 4B). Notably, the deepest erosion of 4.70 m was located in the downstream part of the basin, along banks affected also by windthrows. Conversely, the depositional areas were predominantly located in the middle of the stream and the highest deposit was 3.10 m. The DoD segregation pointed out that all the sub-reaches were eroded and the downstream sub-reach has the highest average net thickness of difference with −0.45 m (Table 3). Therefore, sub-reach 6 presented the highest averaged rate of erosion (averaged to the area of the sub-reach), followed by sub-reaches 3, 4 and 1 with remarkable erosion rates. Differently, sub-reaches 2 and 5 exhibited the lower average net thickness of difference with −0.07 m and −0.08, respectively, stressing that they were closer to balancing the erosional and depositional volumes than other sub-reaches. These results were confirmed in the DoD profile (Fig. 4C), in which the DoD was presented as the sum of all the values hydrologically equidistant from the outlet. Sub-reach 6 exhibited predominant erosion values, whereas sub-reach 2 and 5 showed erosion values almost balanced with deposition ones. As proven by the elevation profile, sub-reach 2 corresponds to a flatter part of the Rio Cordon. The unit stream power acted in each sub-

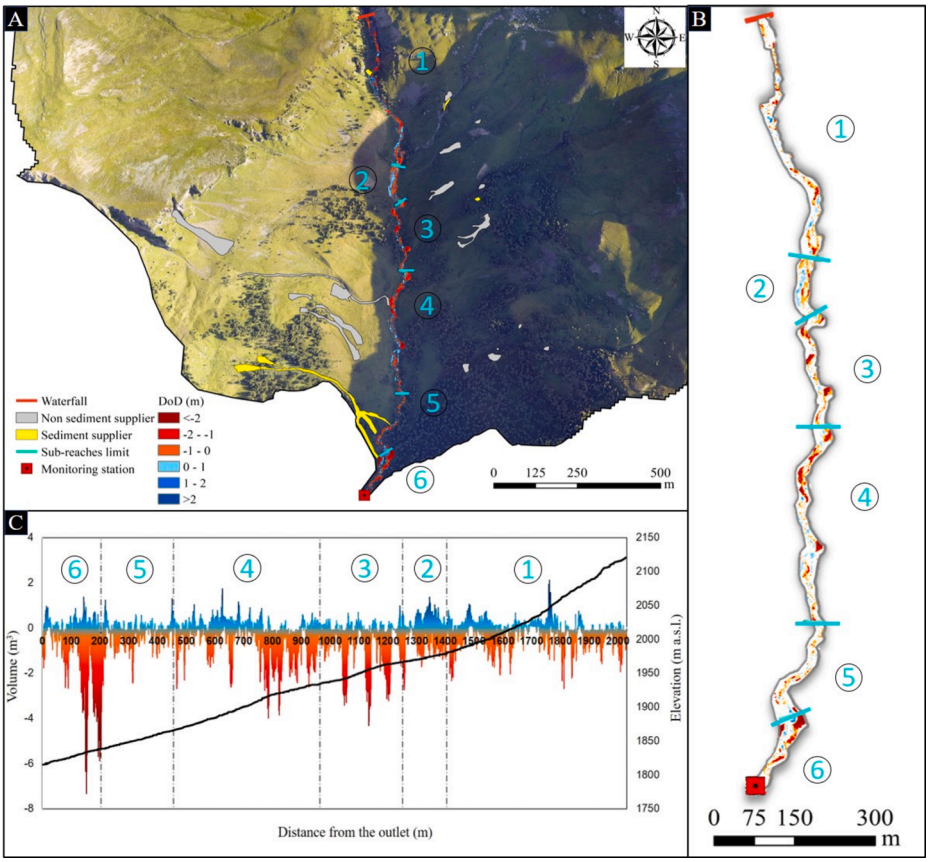

Fig. 4. The geomorphic response of the lower Rio Cordon basin: A) location of the source areas and their potential role as sediment supplier to the active channel (sub-reaches 1–6); B) zoom of the spatial pattern of geomorphic changes along the Rio Cordon obtained from the DoD; C) DoD represented as the sum of eroded (red) and deposited (blue) volume along the longitudinal profile of the active channel.

Table 3
Summary of the results for each sub-reach concerning unit stream power (ω_{Pi}), width ratio (*Wr*) and average net thickness of difference (DoD).

Sub-reach	Contributing area	Length	ω_{Pi}	*Wr*	*DoD*
	(km^2)	(m)	(W m^{-2})		(m)
1	2.30	623	2487	1.21	− 0.12
2	3.37	154	2971	1.79	− 0.07
3	3.50	288	2984	1.39	− 0.24
4	4.28	510	3534	2.44	− 0.19
5	4.47	251	3586	2.01	− 0.08
6	5.00	197	3865	3.76	− 0.45

reach (ω_{Pi}) showed a progressive increase by moving from upstream to downstream, spanning from ω_{P1} = 2487 W m^{-2} to ω_{P6} equal to 3865 W m^{-2}. Interestingly, sub-reach 1 expressed a width ratio (*Wr*) close to 1, while sub-reach 6 experienced major planimetric variations with a *Wr* equal to 3.76 (Table 3). In this sense, the width ratio scaled roughly linearly with the unit stream power (R^2 = 0.749, p-value < 0.05), while a weak relationship was observed between ω_{Pi} and DoD values (R^2 = 0.293, p-value > 0.05). Therefore, the results suggest that stream power variation led to a linear variation in the channel width but not in the streambed elevation.

3.4. Sedimentological effects

The post-flood GSD of Rio Cordon resulted slightly finer than pre-event, with $D_{16}/D_{50}/D_{84}/D_{90}$ that varied from 29/114/358/455 mm, respectively, to 26/78/302/423 mm (Fig. 5). Particularly, it should be stressed the reduction of about a third experienced by D_{50}. The coarse material transported to the monitoring station exhibited a GSD comparable to that expressed by the streambed material, with D_{16} = 38 mm, D_{50} = 90 mm, D_{84} = 248 mm and D_{90} equal to 381 mm (Fig. 5).

The ten largest elements were characterized measuring the axis and, thus, estimating the weight. These boulders had a *b*-axis between 400 and 1100 mm, corresponding to an estimated weight between 0.11 and 1.75 t. Field evidence suggested that these elements were recruited primarily from banks and cascade/step-pool sequences, being then transported for tens of meters. The relationship observed in the period

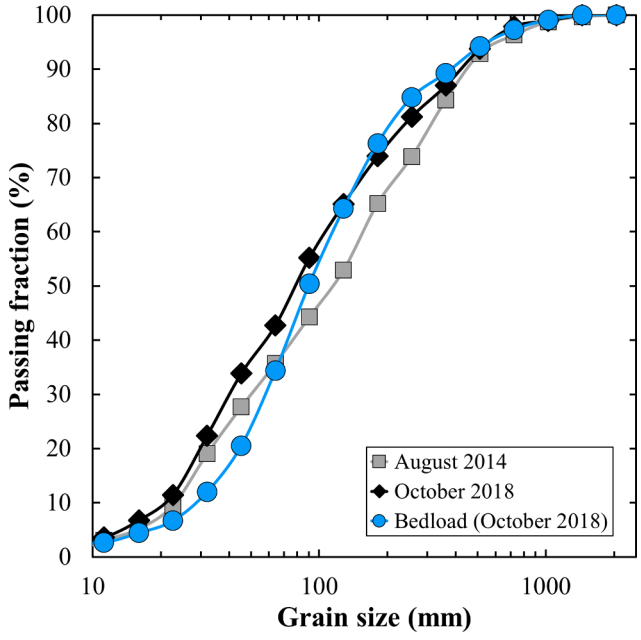

Fig. 5. Comparison between grain size distributions of pre- (August 2014) and post-flood (October 2018) Rio Cordon streambed as well as of October 2018 bedload.

2012–2018 between critical unit water discharge (q_c) and particle size (Rainato et al., 2020) permitted to roughly determine the hydraulic forcing that caused the boulder entrainment. Considering the ten largest elements, the analysis suggested q_c between 0.68 m^2 s^{-1} and 1.51 m^2 s^{-1}.

The bedload storage area located at the measuring station was completely filled with coarse sediment (Fig. 6). In this area, the DoD analysis determined a bedload volume (BL_{Obs}) equal to 6656 m^3 ± 769 m^3, over an extent of about 4200 m^2. Therefore, the average net thickness of difference was 1.58 m, with the maximum elevation change reaching 5.96 m of deposition. The reconstruction of the hydrograph also permitted to determine the bedload volume predicted (BL_{Pred}) by bedload equation. The application of the Schoklitsch (1962) equation suggested a bedload volume of 6890 m^3, of which 32 m^3 were associated to Phase 1 and 6858 m^3 to Phase 2 (Fig. 3). Interestingly, the total 6890 m^3 resulted higher by a factor of 1.04 respect to the *BL* calculated by DoD analysis. Thus, the bedload volume expressed by the October 2018 flood was considered as the average between BL_{Obs} and BL_{Pred}, i.e., equal to about 6800 m^3.

In terms of *BL*, the October 2018 flood appeared the largest event recorded in the last 34 years (1986–2018), resulting greater than the second flood by a factor of ~7.5, i.e., the September 1994 event (*BL* = 900 m^3), and by a factor of 3.68 than the cumulative bedload volume generated by the 33 previous events. Moreover, the bedload was transported over a T_{Bl} of 22 h, corresponding to a transport rate equal to 309 m^3 h^{-1}. In terms of bedload yield, the October 2018 flood delivered 11,713 t of coarse material, accounting for 99% of the annual bedload recorded in 2018 and 79% of total bedload observed in the period 1986–2018 (Fig. 7). Considering this period and accounting the October 2018 event, the Rio Cordon basin therefore exhibited a total sediment yield = 26840 t, which corresponds to a mean sediment yield of 162.6 t km^{-2} y^{-1}. It is worth bearing in mind that this estimate does not account for the suspended sediment load generated by October 2018 event.

Considering the 34 floods recorded in the Rio Cordon basin in the period 1986–2018, it is possible to note a power law relationship between Q_P and *BL* (R^2 = 0.719, p-value < 0.01), in which the October 2018 flood represents the upper bound (Fig. 8a). In addition, the bedload GSD seems to be described by Q_P, with the transported $D_{16}/D_{50}/D_{84}/D_{90}$ well predicted by the peak of water discharge. Notably, the relationship performance increases with the coarsening of the percentiles (Fig. 8b). In fact, the relationships $Q_P - D_{90}$ and $Q_P - D_{84}$ showed R^2 = 0.842 (p-value < 0.01) and R^2 = 0.813 (p-value < 0.01), respectively, with the larger elements mobilized by October 2018 flood. Differently, $Q_P - D_{50}$ (R^2 = 0.677, p-value < 0.01) and $Q_P - D_{16}$ (R^2 = 0.421, p-value < 0.05) resulted more scattered, with October 2018 event that transported D_{50} and D_{16} similar to those entrained by lower magnitude floods. Overall, a progressive increase of both the factor *a* and exponent *b* can be noticed with the coarsening of the percentile considered (Fig. 8b).

The ratio between *BL* (in t) and *ER* expressed by each flood recorded (1986–2018) enabled to investigate the temporal trend of transport efficiency. Fig. 9 shows a general decreasing trend over the long-term period, with most of the events characterized by a *BL/ER* ratio between 0.1 and 10.0. The only floods that clearly deviate from the general trend were the September 1994 (*BL/ER* = 58.0) and the October 2018 (*BL/ER* = 58.3).

4. Discussion

4.1. Rainfall conditions

The heavy precipitation generated in the study basin by the Vaia storm was not continuous but exhibited a hiatus of about 9 h, permitting the identification of a Phase 1 and a Phase 2 in the rainfall event (Table 1). This temporal distribution is consistent to what was shown by Vaia storm over northeastern Italy (Davolio et al., 2020; Giovannini

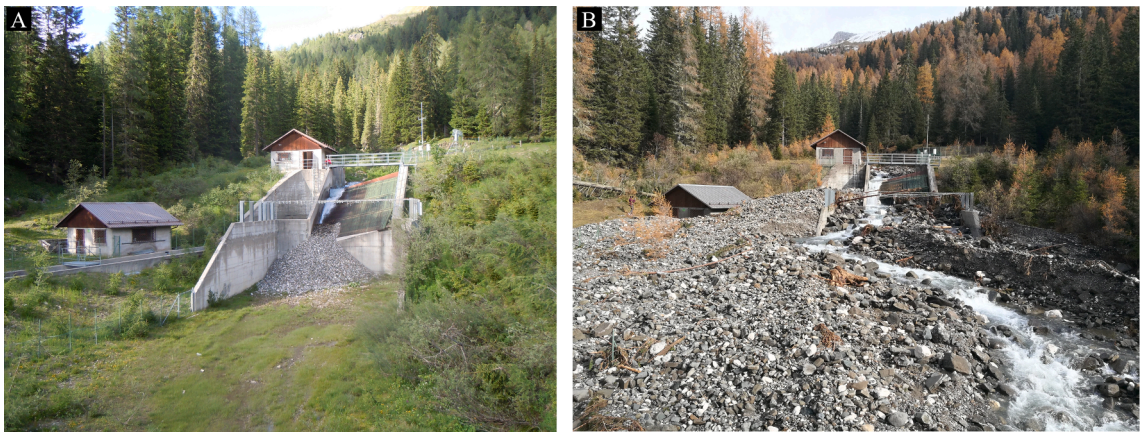

Fig. 6. Bedload storage area (A) pre- and (B) post-October 2018 flood.

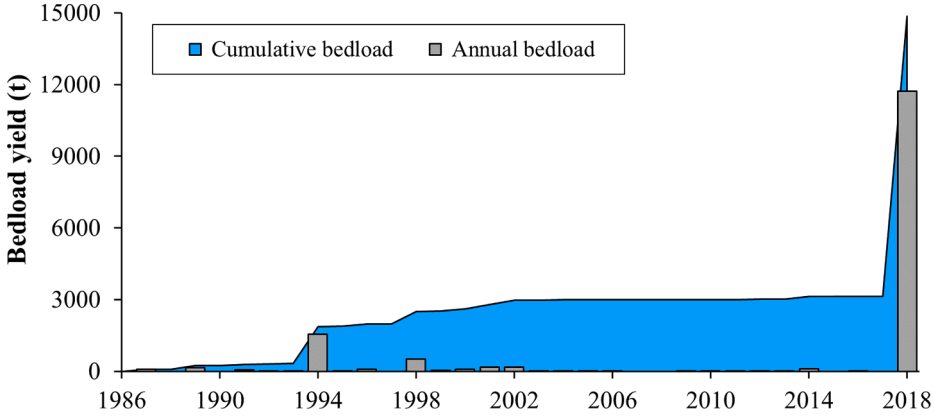

Fig. 7. Annual and cumulative bedload yields in the Rio Cordon between 1986 and 2018.

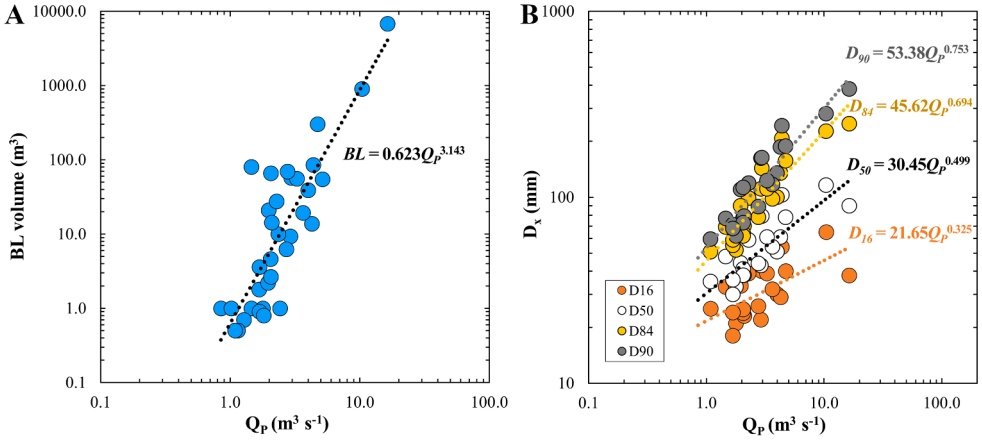

Fig. 8. Relationship between Q_P and (A) *BL* volume, and (B) D_{16}, D_{50}, D_{84}, D_{90}, transported by the 34 flood events recorded in the Rio Cordon (1986–2018). The dotted lines are the best-fit lines for each relationship investigated.

et al., 2021). The maximum rainfall intensities recorded in 5, 15, 30 min (I_{5min}, I_{15min}, I_{30min}) were characterized by $RI < 2$ years, while considering longer time intervals ($I_{6h} - I_{72h}$) the *RI* resulted well over 50 years, emphasizing the persistence of rainfall occurred in the Rio Cordon basin. These results agree with Giovannini et al. (2021) who, investigating the main characteristics of the Vaia storm, reported 72 h accumulated precipitation with $RI > 200$ years in most of the eastern Italian Alps. The moderate but persistent pattern of rainfall was further stressed by the comparison of other high magnitude/low frequency events documented in mountain basins. Batalla et al. (1999) documented, in the Arás basin, a flash flood associated to boulder mobility and massive sediment transport and caused by a brief but intense summer thunderstorm that featured a mean rainfall intensity of 250 mm h^{-1} (Table 4). Similarly, Turowski et al. (2009) analyzed three high magnitude floods that affected the Erlenbach basin with large bedload and boulder mobility, identifying intense summer thunderstorms as triggering factor. These events were characterized by I_{1h} (40.4–61.3 mm) and mean rainfall intensity (12.9–36.8 mm h^{-1}) clearly higher than those observed in the

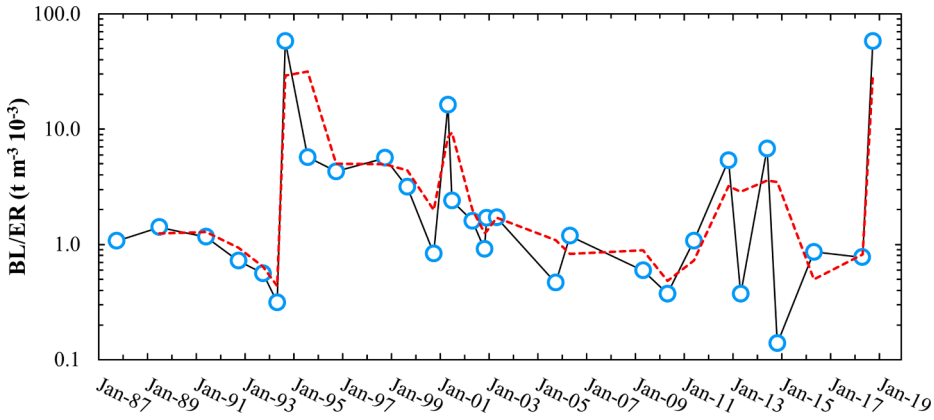

Fig. 9. Temporal trend expressed by the *BL/ER* ratio over the 34 flood events recorded in the Rio Cordon (1986–2018). The red dotted line is the 2-event moving average.

Table 4
Main characteristics of the high magnitude/low frequency event analyzed in this work, compared with those observed in mountain basins by other authors. *A* is the basin area; *S* the mean channel slope; Rainfall description indicates the precipitation type triggering the flood event (PP = persistent precipitation, ST = summer thunderstorm); Basin responses describes the main effects induced by the high magnitude/low frequency event in each study basin (CC = channel changes, BM = boulder mobility, HF = Hyperconcentrated flow, DF = debris flows, LA = landslides).

Study basin	Event	*A* (km^2)	*S* (m m^{-1})	Rainfall description	Mean rainfall intensity (mm h^{-1})	Unit peak discharge (m^3 s^{-1} km^{-2})	Unit stream power (W m^{-2})	Basin responses	Reference
Rio Cordon	October 2018	5.0	0.17	PP	4.4	3.3	2487–3865	CC, BM	This work
Arás	August 1996	18.0	0.14	ST	250.0	20.0	–	CC, HF, BM	Batalla et al. (1999)
Emme	July 2014	94.0	0.02	ST	~87.0	2.7–4.7	–	CC, DF, LA	Ruiz-Villanueva et al. (2018)
Erlenbach	July 1984	0.7	0.18	ST	21.3	17.1	–	CC, BM	Turowski et al. (2009)
Erlenbach	July 1995	0.7	0.18	ST	12.9	14.0	–	CC, BM	Turowski et al. (2009)
Erlenbach	June 2007	0.7	0.18	ST	36.8	20.9	–	CC, BM	Turowski et al. (2009)
Fourmille	September 2013	65.0	0.03[a]	PP	~2.6	–	2500	CC, BM, DF	Wicherski et al. (2017)
Grimmbach	May 2016	30.0	0.02	–	~6.4	22.6–25.1	–	CC, LA	Lucía et al. (2018)
Jamne	July 2018	8.9	–	ST	~2.0	4.6–4.8	770–2769	CC	Bucała-Hrabia et al. (2020)
Jaszcze	July 2018	11.4	–	ST	~2.0	4.1–4.5	767–2703	CC	Bucała-Hrabia et al. (2020)
Orlacher Bach	May 2016	6.0	0.06	–	~6.4	20.0	–	CC, LA	Lucía et al. (2018)
Rio Cordon	September 1994	5.0	0.17	ST	16.0	2.1	–	CC, BM, LA	Lenzi et al. (1999)
Selška Sora	September 2007	29.8	0.02	–	~20.0	4.4	–	CC, DF, LA	Marchi et al. (2009b)
Tegnas	October 2018	52.0	0.03	PP	5.7	3.3	–	CC, DF, LA	Pellegrini et al. (2021)

[a] Averaged value.

Rio Cordon basin during the Vaia storm, but associated to a total precipitation (45.3–106.7 mm) and a total precipitation duration (1.5–5.0 h) notably lower. Few authors described high magnitude/low frequency events triggered by persistent precipitation. In the Fella River basin, Marchi et al. (2009a) analyzed a convective storm (I_{12h} = 390 mm) which caused a massive debris flow with a mobilized volume of ~78,000 m^3, while a 6 days rainfall event with a total precipitation of 501.0 mm and daily rainfall between 27.2 and 246.4 mm led to a flood with *RI* > 200 years in the Ligurian Alps (Nannoni et al., 2020).

4.2. Hydraulic forcing

The use of indirect methods to estimate the hydraulic forcing acted in the Rio Cordon led to an implicit uncertainty, which needs to be considered. In fact, the hydrograph reconstruction was based on the use of the discharge measured in the Fiorentina basin to describe what occurred in the Rio Cordon sub-basin. The $Q_{Fi} - Q_{Rc}$ relationship was statistically significant and based on 1762 discharge measurements recorded during floods triggered by persistent precipitation, i.e., same rainfall conditions that led to the October 2018 flood. However, it is worth noting that these floods were near-bankfull events and, therefore, the $Q_{Fi} - Q_{Rc}$ relationship may have allowed a better description of under- and near-bankfull discharge than over-bankfull conditions. Nevertheless, the reconstructed hydrograph seems reliable since it reflected the temporal distribution of rainfall registered. Thus, specific analyses were made to determine the corresponding Q_P using the slope conveyance method (Gaume and Borga, 2008) and the basin area scaling ratio proposed by Bravard and Petit (1997). This latter indirect method is characterized by an implicit source of uncertainty due to the basin to sub-basin discharge extrapolation. This uncertainty may have been

somewhat reduced by means of the site specific coefficient *c* (see Section 2.3) already used and tested in the Rio Cordon (Oss Cazzador et al., 2021). Thus, the Q_P inferred for Phase 1 (2.87 ± 0.56 $m^3 s^{-1}$) and Phase 2 (16.36 ± 1.14 $m^3 s^{-1}$) were associated to the hydrograph reconstructed and, in particular, in the Phase 2 the hydrograph was integrated by a part simulated to describe the peaking portion of flood. This simulated part involved 3 h of the 90 h investigated (October 27th–October 30th) and it was described as a triangular shape according to the hydrograph shape observed in mountain basins during high magnitude/low frequency floods (Lenzi et al., 1999; Marchi et al., 2009a; Turowski et al., 2009). Interestingly, this shape was consistent to the hydrograph generated by the Vaia storm in another basin of eastern Italian Alps, i.e., the Tegnas catchment (Pellegrini et al., 2021). The hydraulic forcing conditions estimated clearly stressed the high magnitude expressed by the October 2018 flood event (Table 2). This high magnitude can be ascribed to the amount and intensity of rainfall but also to their temporal distribution and soil moisture. The soil conditions may have also influenced the perifluvial areas, where important windthrows were observed (Picco et al., 2020) likely to the high wind gusts of October 29th acting on a saturated and softened terrain.

In the Rio Cordon, the October 2018 flood resulted in a unit peak discharge of 3.3 $m^3 s^{-1} km^{-2}$. This value was lower than those described in the Erlenbach by Turowski et al. (2009), who observed a unit peak discharge between 14.0 and 20.9 $m^3 s^{-1} km^{-2}$ in large floods due to intense thunderstorms (Table 4). Higher unit peak discharges were documented even in the Fella River basin by Marchi et al. (2009a) and in Grimmbach and Orlacher Bach by Lucía et al. (2018), who reported 20.0 $m^3 s^{-1} km^{-2}$ and 20.0–25.1 $m^3 s^{-1} km^{-2}$, respectively. Hydraulic forcing comparable to that observed in the Rio Cordon were detected by Marchi et al. (2009b) in the Selška Sora basin, where a flash flood expressed 4.4 $m^3 s^{-1} km^{-2}$, and by Ruiz-Villanueva et al. (2018) that reported a unit peak discharges between 2.7 and 4.7 $m^3 s^{-1} km^{-2}$ ascribed to heavy and extensive summer precipitation in the Emme River basin (Table 4). Particularly, the unit peak discharge calculated in the Rio Cordon resulted consistent to the 3.3 $m^3 s^{-1} km^{-2}$ experienced in the Tegnas catchment during the Vaia storm (Pellegrini et al., 2021). Also, the peaks of unit stream power inferred along the main channel ($\omega_{P1\text{-}6}$ = 2487–3865 W m^{-2}) appeared comparable, although at the upper limit, to those reported in literature. In fact, the small Jamne and Jaszcze basins, located in the Western Polish Carpathians, experienced ω between 767 and 2769 W m^{-2} as a consequence of flood due to heavy summer precipitation (Bucała-Hrabia et al., 2020). In Fourmille Creek, Wicherski et al. (2017) documented a precipitation event of 350 mm in seven days, which generated over-bankfull discharge for 120 h and a maximum ω of about 2500 W m^{-2} (Table 4). Instead, the range of unit stream power determined in the Rio Cordon appeared in line to what observed by Yochum et al. (2017) in the Colorado Front Range as consequence of persistent heavy rainfall (~460 mm in 10 days). These authors analyzed 531 stream reaches, estimating maximum ω between 30 and 7000 W m^{-2}.

4.3. Hillslopes and main channel responses

The limited response of hillslope and the only 26 sediment sources (re)activated could be attributed to the moderate rainfall intensity that, in combination with the hiatus in precipitation, may have precluded an extensive slope instability. Also, the lack of other high magnitude events in the period 1994–2018, might have reduced the erosional processes and favored a consequent stabilization trend along the hillslopes (Ferrato et al., 2017). Differently, in the Tegnas catchment characterized by a similar geological substrate, the Vaia storm caused a marked increase of sediment sources with the catchment area covered by instabilities, such as debris flows and landslides, augmented from 0.33% to 0.83% (Pellegrini et al., 2021), whereas in the Rio Cordon basin this extent increased only from 0.13% to 0.14%. The sediment sources were investigated as potential suppliers in the lower basin. According to Dalla Fontana and Marchi (1994), the lower Rio Cordon belt shows predominant erosion areas (e.g., landslides, debris flows, stream bank erosions), where the sources are potentially more capable of transferring sediment to the downstream outlet in respect to the upper basin (Cavalli et al., 2016). In this sense, recent analyses performed on the upper plateau by Oss Cazzador et al. (2021) demonstrated that, although the October 2018 flood caused the reconfiguration of the upper reach (estimated *BL* = 86.0–133.2 m^3), it did not effectively transferred sediment to the downstream part of the basin. According to the IC-DoD analysis, only few sources acted as sediment suppliers to the main active channel during the event. Although it proved to be sufficiently reliable, this approach can be further improved. First, the DoD should consider more frequent surveys, second the IC analysis could involve a deeper and extensive field analysis to derive a more accurate threshold (see Section 2.4.3). However, the analyses stressed that the Rio Cordon basin showed evidence of limited lateral connectivity, since only few sediment sources supplied material to the channel network. On the contrary, it showed high longitudinal connectivity due to the evident linkage between active channel and outlet (Fryirs et al., 2007). The DoD analysis suggested that the moderate but persistent rainfall caused greater hydraulic forcing along the main channel than along the slopes, leading to a predominant alluvial response of the Rio Cordon basin. This hypothesis was supported by a volume eroded from Rio Cordon (6979 m^3) clearly larger than the potential volume supplied by sediment sources (1140 m^3). In fact, the DoD pointed out that along the active channel the October 2018 flood resulted in severe erosion processes, with large streambed incisions and banks scouring. Particularly, an evident widening was observed along the 2023 m analyzed, with the average channel width that varied from 6.30 m, pre-event, to 10.60 m post-event. In this sense, it is worth noting that the geomorphic changes measured can be affected by uncertainty due to: (i) the error range in the active channel DoD, corresponding to ±2059 m^3 (29.5%); (ii) the inaccuracies related to the channel width measuring by means of orthophotos interpretation. Despite these sources of uncertainty, the results seem to suggest that the sediment transport benefited by quasi-unlimited sediment supply conditions mainly due to an extensive alteration of active channel, where the armoured layer was removed. From the DoD analysis a longitudinal pattern along the channel was hardly detectable as many avulsions caused the variation of the stream pathway and no clear erosional/depositional alternation can be used to infer in-channel sediment transfers (Calle et al., 2020). However, the subdivision in sub-reaches helped to reconstruct the linkage between the hydraulic forcing and the geomorphic response. As supported by Marchi et al. (2016), unit stream power was able to describe the major geomorphic changes at channel reach scale. In particular, consistency between ω_{Pi} and lateral geomorphic changes (*Wr*), rather than vertical (DoD), was found. This result appeared in line with Krapesch et al. (2011), who successfully predicted channel widening, caused by extreme floods in alpine gravel bed rivers, by using ω determined by means of the pre-event channel width. In the Rio Cordon basin, the definition of the hydraulic forcing conditions and the induced geomorphic changes supported also the hypothesis that the high magnitude/low frequency floods are the only events that can severely alter the rough boulder streams (Baker and Costa, 1987).

4.4. Sedimentological response

The hydraulic forcing and erosive processes triggered by October 2018 flood resulted in a massive sediment transport. The GSD investigation stressed that the entire streambed grain size, from fine gravel to large boulders, was mobilized (Fig. 5). This finding supports the hypothesis that the Rio Cordon experienced structural bedload, condition under which a complete streambed remobilization occurred (Piton and Recking, 2017). Consistently, the mobility of large boulders was also observed, highlighting the outstanding hydraulic forcing expressed by October 2018 event. In this sense, it is interesting to note that, in literature, the transport of boulders was generally documented for higher

unit peak discharges (Table 4). However, Wicherski et al. (2017) observed boulder mobility in the Fourmille Creek as a consequence of ω comparable to that exerted in the Rio Cordon by October 2018 flood. Therefore, these outcomes stressed out the need to better comprehend the boulder mobility, a condition that can strongly impact the mountain streams but that was only rarely investigated. The approaches used to determine the bedload volume, i.e., DoD analysis and bedload prediction, provided very similar volumes, with a BL_{Obs}/BL_{Pred} ratio equal to 0.97. In the Rio Cordon, this ratio was always lower due to the overestimation of BL_{Pred} by Schoklitsch (1962) equation and, in general, by bedload equations, with respect to BL_{Obs} (D'Agostino and Lenzi, 1999; Rainato et al., 2017). Therefore, the good match between BL_{Obs} and BL_{Pred} emphasized the high hydraulic forcing of October 2018 flood coupled with a high sediment supply, conditions under which the bedload equations can provide the highest predictive performance (D'Agostino and Lenzi, 1999; Recking, 2012; Rickenmann, 2020). However, it is worth noting that both BL_{Pred} and BL_{Obs} might be affected by a certain degree of uncertainty. On the one hand, BL_{Pred} was calculated by means of the Schoklitsch equation applied to the hydrograph reconstructed (see Section 4.2). Therefore, the intrinsic uncertainty affecting the discharges estimated may have propagated in the predicted bedload. On the other hand, the BL_{Obs} determined by DoD analysis presented an error range of ± 769 m^3, corresponding to about 11.5% of the volume observed. Finally, BL_{Obs} might be affected by a partial underestimation as the October 2018 flood caused the complete filling of the bedload storage area, up to its maximum capacity (Fig. 6), and therefore a certain portion of bedload may have been transported further downstream.

4.5. Large and infrequent floods in Rio Cordon basin

The two high magnitude/low frequency floods occurred in the catchment were caused by markedly different rainfall conditions. The intense summer thunderstorm that triggered the September 1994 flash flood exhibited $I_{5min}/I_{15min}/I_{30min}$ about twice the Vaia storm's values but lasted 12 h, i.e., a total precipitation duration considerably shorter than the 79.8 h estimated in October 2018 (Table 1). The prolonged rainfalls of October 2018 produced the highest hydraulic forcing conditions among the 34 floods recorded in the Rio Cordon since 1986 (Supplementary S1). Particularly, the estimated water discharge peak ($Q_P = 16.36 \pm 1.14$ m^3 s^{-1}) and effective runoff ($ER = 201.0 \times 10^3$ m^3) were higher by a factor of 1.57 and 7.56, respectively, than those exhibited by September 1994 flood. Despite this outstanding hydraulic forcing, the hillslope response to the October 2018 event was modest. In particular, the number of newly formed sediment source areas was relatively low compared to what produced by the September 1994 flood (Dalla Fontana and Marchi, 1994; Lenzi and Marchi, 2000). This diverse response appears to be due to the different rainfall intensity showed by the flood events (Table 4). However, in both high magnitude/low frequency floods, the main sediment source was identified in the active channel and, particularly, in the streambed that experienced armoured layer removal. In October 2018, the alteration faced by the main channel was clearly larger than in 1994, with unprecedented lateral widenings and avulsions. This finding confirmed that, with similar unit stream power and peak discharge, long-lasting floods can produce larger geomorphic changes than flash floods (Costa and O'Connor, 1995; Magilligan et al., 2015; Marchi et al., 2016). The hydraulic and geomorphic forcing exerted by October 2018 flood triggered boulder mobility in the Rio Cordon main channel, a condition that was previously observed only in the September 1994 event. In this sense, according to Rainato et al. (2020), the largest element (*b-axis* = 1100 mm) recovered in the bedload storage area after the October 2018 flood suggests a critical unit water discharge (q_c) of 1.51 m^2 s^{-1}, thus, higher than $q_c = 1.25$ m^2 s^{-1} observed in the September 1994 flood (Lenzi et al., 2006b). Also in terms of bedload volume, the October 2018 flood ($BL = 6800$ m^3) was the largest event recorded in the Rio Cordon basin, and about one order of magnitude larger than the September 1994 event ($BL = 900$ m^3). Interestingly, the two high magnitude/low frequency events showed comparable transport rate, i.e., 309 m^3 h^{-1} in October 2018 flood and 323 m^3 h^{-1} in September 1994 event but the latter lasted 3 h, while, during the former, bedload persisted 22 h. The *BL* magnitude expressed by October 2018 flood was also clearly noticeable in terms of sediment yield, accounting for 79% of the total bedload delivered during the period 1986–2018 and, then, leading to an abrupt increase over the annual trend (Fig. 7). In light of climate change, because of which a higher frequency of heavy rainfall event is expected (Fischer and Knutti, 2015; Peleg et al., 2020), the observed relationships Q_P-*BL* volume and Q_P-GSD transported seem to suggest that in the near future, in the Rio Cordon, other massive bedload transport accompanied by the mobilization of coarse grain size could be awaited. Additionally, the October 2018 flood induced a peak in the temporal trend of *BL/ER* ratio, similarly to what was caused by the September 1994 event, i.e., a condition that favoured about a decade of increased transport efficiency (Rainato et al., 2017).

5. Conclusions

In alpine basins, severe rainfall events and induced large floods can influence erosion processes, sediment dynamics and landscape evolution over large spatial and temporal scales. However, given the high magnitude/low frequency, these events and their effects are difficult to measure and, thus, to be documented. Additionally, even rarer are the studies proposing a comprehensive approach that encompasses all the main responses to the events. This work analyzed the hydrological, geomorphic and sedimentological responses of an alpine basin (Rio Cordon basin) to the Vaia storm, a severe weather event that affected northeastern Italy in October 2018. In the Rio Cordon basin, the Vaia storm resulted as a severe and persistent rainfall event, during which the rainfall intensities for sub-hourly intervals were ordinary, while for longer time intervals expressed $RI > 50$ years. The combination of different indirect methods helped the hydraulic forcing quantification. Despite the uncertainty associated to this approach, the analyses clearly stressed the outstanding hydraulic forcing occurred during the flood, pointing out the largest Q_P and *ER* ever recorded in 34 years. These conditions induced a moderate hillslope response, with only few new sediment sources capable of acting as sediment suppliers to the main channel. Instead, the precipitation favored a predominant alluvial response of the basin, with the Rio Cordon severely altered by lateral widening, deep streambed incision and armouring removal. In terms of sedimentological response, the hydraulic forcing and the erosive processes induced by the Vaia storm resulted in streambed remobilization, boulder mobility and in a bedload volume about four times the one produced cumulatively by the 33 previous events. Thanks to a monitoring program maintained over three decades, the Rio Cordon basin offered the uncommon chance to compare characteristics and effects of two high magnitude/low frequency floods. These two events exhibited different rainfall and hydraulic forcing conditions that favored in the September 1994 flash flood a hillslope response larger than in the October 2018 event, which instead altered the main channel more extensively. These conditions resulted in a different sedimentological response of the basin, clearly evident in terms of bedload volume, supporting the hypothesis that floods featuring high Q_P (or ω_P) combined with a long duration can severely influence the mountain fluvial systems. Therefore, bearing in mind the long-lasting effects induced by the previous large and infrequent event, what can be expected for the future? Has the October 2018 event represented the new ground zero for the Rio Cordon basin? To answer these questions, also in the framework of climate change, it will be fundamental to continue investigating over the long-term this and other alpine basins to understand how they will respond to forthcoming ordinary and high magnitude/low frequency events.

Declaration of Competing Interest

The authors declare that they have no known competing financial interests or personal relationships that could have appeared to influence the work reported in this paper.

Acknowledgements

This research was funded by the University of Padova Research Project "Sediment dynamics in alpine environment: analysis of sediment mobility, propagation velocity and bedload magnitude in high gradient streams" [BIRD185008]. We thank the ARPA Veneto for providing raw rainfall data and discharge measurements of Fiorentina Stream. We would like to thank Daniele Oss Cazzador for his help in the field activities and Prof. Mario Aristide Lenzi for his valuable suggestions and comments. Finally, we thank the Co Editor-in-Chief Markus Egli, the Associate Editor Jantiene Baartman and two anonymous reviewers for their constructive comments, which improved the quality of the manuscript.

Appendix A. Supplementary data

Supplementary data to this article can be found online at https://doi.org/10.1016/j.catena.2021.105600.

References

Amponsah, W.A., Ayral, P.A., Boudevillain, B.B., Bouvier, C., Braud, I., Brunet, P., Delrieu, G., Didon-Lescot, J.F., Gaume, E., Lebouc, L., Marchi, L., Marra, F., Morin, E., Nord, G., Payrastre, O., Zoccatelli, D., Borga, M., 2018. Integrated high-resolution dataset of high-intensity European and Mediterranean flash floods. Earth Syst. Sci. Data 10, 1783–1794.

Baewert, H., Morche, D., 2014. Coarse sediment dynamics in a proglacial fluvial system (Fagge River, Tyrol). Geomorphology 218, 88–97.

Baker, V.R., Costa, J.E., 1987. Flood power. In: Mayer, L., Nash, D. (Eds.), Catastrophic Flooding. Allen & Unwin, Boston, pp. 1–20.

Batalla, R.J., De Jong, C., Ergenzinger, P., Sala, M., 1999. Field observations on hyperconcentrated flows in mountain torrents. Earth Surf. Proc. Land. 24, 247–253.

Bauch, G.D., Hickin, E.J., 2011. Rate of floodplain reworking in response to increasing storm-induced floods, Squamish River, south-western British Columbia, Canada. Earth Surf. Proc. Land. 36 (7), 872–884.

Biolchi, S., Denamiel, C., Devoto, S., Korbar, T., Macovaz, V., Scicchitano, G., Vilibić, I., Furlani, S., 2019. Impact of the October 2018 Storm Vaia on coastal boulders in the Northern Adriatic Sea. Water 11 (11), 2229.

Bohorquez, P., Darby, S.E., 2008. The use of one- and two-dimensional hydraulic modelling to reconstruct a glacial outburst flood in a steep Alpine valley. J. Hydrol. 361 (3–4), 240–261.

Borga, M., Stoffel, M., Marchi, L., Marra, F., Matthias, J., 2014. Hydrogeomorphic response to extreme rainfall in headwater systems: flash floods and debris flows. J. Hydrol. 518, 194–205.

Brasington, J., Rumsby, B.T., McVey, R.A., 2000. Monitoring and modelling morphological change in a braided gravel-bed river using high-resolution GPS-based survey. Earth Surf. Proc. Land. 25, 973–990.

Brasington, J., Langham, J., Rumsby, B., 2003. Methodological sensitivity of morphometric estimates of coarse fluvial sediment transport. Geomorphology 53, 299–316.

Bravard, J.P., Petit, F., 1997. Les cours d'eau. In: Dynamique du système fluvial. Armand Colin, Paris, p. 222.

Brierley, G., Fryirs, K., Jain, V., 2006. Landscape connectivity: The geographic basis of geomorphic applications. Area 38 (2), 165–174. https://doi.org/10.1111/j.1475-4762.2006.00671.x.

Brogan, D.J., MacDonald, L.H., Nelson, P.A., Morgan, J.A., 2019. Geomorphic complexity and sensitivity in channels to fire and floods in mountain catchments. Geomorphology 337, 53–68.

Bucała-Hrabia, A., Kijowska-Strugała, M., Bryndal, T., Cebulski, J., Kiszka, K., Kroczak, R., 2020. An integrated approach for investigating geomorphic changes due to flash flooding in two small stream channels (Western Polish Carpathians). J. Hydrol.: Reg. Stud. 31, 100731.

Burt, T.P., Allison, R.J., 2010. Sediment Cascades: An Integrated Approach. John Wiley & Sons, Ltd, Chichester, UK.

Calle, M., Calle, J., Alho, P., Benito, G., 2020. Inferring sediment transfers and functional connectivity of rivers from repeat topographic surveys. Earth Surf. Proc. Land. 45, 681–693. https://doi.org/10.1002/esp.4765.

Carrivick, J.L., Smith, M.W., Quincey, D.J., 2016. Structure from Motion in the Geosciences. John Wiley & Sons Ltd, Chichester, UK.

Cassandro, C., Loglisci, N., Gandini, D., Qian, M.W., Niu, G.Y., Ramieri, P., Pelosini, R., Longhetto, A., 2002. The flood of November 1994 in Piedmont, Italy: A quantitative analysis and simulation. Hydrol. Process. 16, 1275–1299.

Cavaleri, L., Bajo, M., Barbariol, F., Bastianini, M., Benetazzo, A., Bertotti, L., Chiggiato, J., Davolio, S., Ferrarin, C., Magnusson, L., Papa, A., Pezzutto, P., Pomaro, A., Umgiesser, G., 2019. The October 29, 2018 storm in northern Italy – an exceptional event and its modeling. Prog. Oceanogr. 178, 102178.

Cavalli, M., Marchi, L., 2008. Characterisation of the surface morphology of an alpine alluvial fan using airborne LiDAR. Nat. Hazards Earth Syst. Sci. 8, 323–333.

Cavalli, M., Trevisani, S., Comiti, F., Marchi, L., 2013. Geomorphometric assessment of spatial sediment connectivity in small Alpine catchments. Geomorphology 188, 31–41. https://doi.org/10.1016/j.geomorph.2012.05.007.

Cavalli, M., Tarolli, P., Dalla Fontana, G., Marchi, L., 2016. Multi-temporal analysis of sediment source areas and sediment connectivity in the Rio Cordon catchment (Dolomites). Rendiconti Online Società Geologica Italiana 39 (April), 27–30. https://doi.org/10.3301/ROL.2016.39.

Costa, J.E., O'Connor, J.E., 1995. Geomorphologically effective floods. In: Costa, J.E., Miller, A.J., Potter, K.P., Wilcock, P.R. (Eds.), Natural and Anthropogenic Influences in Fluvial Geomorphology (The Wolman Volume) AGU Geophysical Monograph 89. American Geophysical Union, Washington, D.C., pp. 45–56

Crema, S., Cavalli, M., 2018. SedInConnect: a stand-alone, free and open source tool for the assessment of sediment connectivity. Comput. Geosci. 111, 39–45. https://doi.org/10.1016/j.cageo.2017.10.009.

Cucchiaro, S., Cavalli, M., Vericat, D., Crema, S., Llena, M., Beinat, A., Marchi, L., Cazorzi, F., 2019. Geomorphic effectiveness of check dams in a debris-flow catchment using multi-temporal topographic surveys. Catena 174, 73–83.

Cucchiaro, S., Maset, E., Cavalli, M., Crema, S., Marchi, L., Beinat, A., Cazorzi, F., 2020. How does co-registration affect geomorphic change estimates in multi-temporal surveys? GIScience Remote Sens. 57 (5), 611–632. https://doi.org/10.1080/15481603.2020.1763048.

D'Agostino, V., Lenzi, M.A., 1999. Bedload transport in the instrumented catchment of the Rio Cordon: Part II: Analysis of the bedload rate. Catena 36, 191–204.

Dalla Fontana, G., Marchi, L., 1994. Sediment source areas in a small alpine basin. International Symposium on Forest Hydrology, October 24–28, Tokyo, Japan, 455–462.

Davolio, S., Della Fera, S., Laviola, S., Miglietta, M.M., Levizzani, V., 2020. Heavy precipitation over Italy from the Mediterranean storm "Vaia" in October 2018: Assessing the role of an atmospheric river. Mon. Weather Rev. 148, 3571–3588.

Ferrato, C., De Marco, J., Tarolli, P., Cavalli, M., 2017. An updated source areas inventory in the Rio Cordon catchment (Dolomites). Rendiconti Online Società Geologica Italiana 42, 10–13.

Fischer, E.M., Knutti, R., 2015. Anthropogenic contribution to global occurrence of heavy-precipitation and high-temperature extremes. Nat. Clim. Change 5, 560–564.

Friele, P., Millard, T.H., Mitchell, A., Allstadt, K.E., Menounos, B., Geertsema, M., Clague, J.J., 2020. Observations on the May 2019 Joffre Peak landslides, British Columbia. Landslides 17 (4), 913–930.

Fryirs, K.A., Brierley, G.J., Preston, N.J., Kasai, M., 2007. Buffers, barriers and blankets: The (dis)connectivity of catchment-scale sediment cascades. Catena 70 (1), 49–67. https://doi.org/10.1016/j.catena.2006.07.007.

Fryirs, K., 2013. (Dis)Connectivity in catchment sediment cascades: A fresh look at the sediment delivery problem. Earth Surf. Proc. Land. 38 (1), 30–46. https://doi.org/10.1002/esp.3242.

Gaume, E., Borga, M., 2008. Post-flood field investigations in upland catchments after major flash floods: proposal of a methodology and illustrations. J. Flood Risk Manage. 1, 175–189.

Giovannini, L., Davolio, S., Zaramella, M., Zardi, D., Borga, M., 2021. Multi-model convection-resolving simulations of the October 2018 Vaia storm over Northeastern Italy. Atmos. Res. 253, 105455.

Gob, F., Bravard, J.P., Petit, F., 2010. The influence of sediment size, relative grain size and channel slope on initiation of sediment motion in boulder bed rivers. A lichenometric study. Earth Surf. Proc. Land. 35, 1535–1547.

Gorczyca, E., Krzemień, K., Wrońska-Wałach, D., Sobucki, M., 2013. Channel changes due to extreme rainfalls in the Polish Carpathians. In: Loczy, D. (Ed.), Geomorphological Impacts of Extreme Weather, Case Studies from Central and Eastern Europe. Springer, Dordrecht, pp. 23–35.

Hajdukiewicz, H., Wyżga, B., Mikuś, P., Zawiejska, J., Radecki-Pawlik, A., 2016. Impact of a large flood on mountain river habitats, channel morphology, and valley infrastructure. Geomorphology 272, 55–67.

Heckmann, T., Schwanghart, W., 2013. Geomorphic coupling and sediment connectivity in an alpine catchment - Exploring sediment cascades using graph theory. Geomorphology 182, 89–103. https://doi.org/10.1016/j.geomorph.2012.10.033.

Korup, O., 2005. Geomorphic imprint of landslides on alpine river systems, southwest New Zealand. Earth Sur. Proc. Land. 30 (7), 783–800.

Krapesch, G., Hauer, C., Habersack, H., 2011. Scale orientated analysis of river width changes due to extreme flood hazards. Nat. Hazards Earth Syst. Sci. 11, 2137–2147.

Lane, S.N., Westaway, R.M., Hicks, D.M., 2003. Estimation of erosion and deposition volumes in a large, gravel-bed, braided river using synoptic remote sensing. Earth Surf. Proc. Land. 28 (3), 249–271. https://doi.org/10.1002/esp.483.

Lenzi, M.A., 2001. Step-pool evolution in the Rio Cordon, Northeastern Italy. Earth Surf. Proc. Land. 26 (9), 991–1008. https://doi.org/10.1002/esp.239.

Lenzi, M.A., Marchi, L., 2000. Suspended sediment load during floods in a small stream of the Dolomites (northeastern Italy). Catena 39 (4), 267–282. https://doi.org/10.1016/S0341-8162(00)00079-5.

Lenzi, M.A., D'Agostino, V., Billi, P., 1999. Bedload transport in the instrumented catchment of the Rio Cordon: Part I: Analysis of bedload records, conditions and threshold of bedload entrainment. Catena 36 (3), 171–190.

Lenzi, M.A., Mao, L., Comiti, F., 2006a. Effective discharge for sediment transport in a mountain river: computational approaches and geomorphic effectiveness. J. Hydrol. 326 (1–4), 257–276.

Lenzi, M.A., Mao, L., Comiti, F., 2006b. When does bedload transport begin in steep boulder-bed streams? Hydrol. Process. 20, 3517–3533.
Liébault, F., Piégay, H., 2002. Causes of the 20th century channel narrowing in mountain and piedmont rivers of southeastern France. Earth Surf. Proc. Land. 27, 425–444.
Liébault, F., Bellot, H., Chapuis, M., Klotz, S., Deschâtres, M., 2012. Bedload tracing in a high-sediment-load mountain stream. Earth Surf. Proc. Land. 37, 385–399.
Lucía, A., Schwientek, M., Eberle, J., Zarfl, C., 2018. Planform changes and large wood dynamics in two torrents during a severe flash flood in Braunsbach, Germany 2016. Sci. Total Environ. 640–641, 315–326.
Magilligan, F.J., 1992. Thresholds and the spatial variability of flood power during extreme floods. Geomorphology 5, 373–390.
Magilligan, F.J., Buraas, E.M., Renshaw, C.E., 2015. The efficacy of stream power and flow duration on geomorphic responses to catastrophic flooding. Geomorphology 228, 175–188.
Mao, L., Lenzi, M.A., 2007. Sediment mobility and bedload transport conditions in an alpine stream. Hydrol. Process. 21, 1882–1891.
Marchi, L., Cavalli, M., Sangati, M., Borga, M., 2009a. Hydrometeorological controls and erosive response of an extreme alpine debris flow. Hydrol. Process. 23 (19), 2714–2727.
Marchi, L., Borga, M., Preciso, E., Sangati, M., Gaume, E., Bain, V., Delrieu, G., Bonnifait, L., Pogačnik, N., 2009b. Comprehensive post-event survey of a flash flood in Western Slovenia: observation strategy and lessons learned. Hydrol. Process. 23, 3761–3770.
Marchi, L., Cavalli, M., Amponsah, W., Borga, M., Crema, S., 2016. Upper limits of flash flood stream power in Europe. Geomorphology 272 (1), 68–77.
McEwen, L.J., Werritty, A., 1988. The hydrology and long-term geomorphic significance of a flash flood in the Cairngorm mountains, Scotland. Catena 15, 361–377.
Messenzehl, K., Hoffmann, T., Dikau, R., 2014. Sediment connectivity in the high-alpine valley of Val Müschauns, Swiss National Park - linking geomorphic field mapping with geomorphometric modelling. Geomorphology 221, 215–229. https://doi.org/10.1016/j.geomorph.2014.05.033.
Miller, A.J., 1990. Flood hydrology and geomorphic effectiveness in the central Appalachians. Earth Surf. Proc. Land. 15, 119–134.
Montgomery, D.R., Buffington, J.M., 1997. Channel-reach morphology in mountain drainage basins. Geol. Soc. Am. Bull. 109 (5), 596–611.
Nannoni, A., Vigna, B., Fiorucci, A., Antonellini, M., De Waele, J., 2020. Effects of an extreme flood event on an alpine karst system. J. Hydrol. 590, 125493.
Oss Cazzador, D., Rainato, R., Cavalli, M., Lenzi, M.A., Picco, L., 2020. Integrated analysis of sediment source areas in an Alpine basin. Catena 188, 104416. https://doi.org/10.1016/j.catena.2019.104416.
Oss Cazzador, D., Rainato, R., Mao, L., Martini, L., Picco, L., 2021. Coarse sediment transfer and geomorphic changes in an alpine headwater stream. Geomorphology 376, 107569. https://doi.org/10.1016/j.geomorph.2020.107569.
Pagano, S.G., Rainato, R., Garcia-Rama, A., Gentile, F., Lenzi, M.A., 2019. Analysis of suspended sediment dynamics at event scale: comparison between a Mediterranean and an Alpine basin. Hydrol. Sci. J. 64 (8), 948–961.
Pastorello, R., D'Agostino, V., Hürlimann, M., 2020. Debris flow triggering characterization through a comparative analysis among different mountain catchments. Catena 186, 104348. https://doi.org/10.1016/j.catena.2019.104348.
Peleg, N., Skinner, C., Fatichi, S., Molnar, P., 2020. Temperature effects on the spatial structure of heavy rainfall modify catchment hydro-morphological response. Earth Surf. Dyn. 8, 17–36.
Pellegrini, G., Martini, L., Cavalli, M., Rainato, R., Cazorzi, A., Picco, L., 2021. The morphological response of the Tegnas alpine catchment (Northeast Italy) to a Large Infrequent Disturbance. Sci. Total Environ. 770, 145209 https://doi.org/10.1016/j.scitotenv.2021.145209.
Picco, L., Rainato, R., Pellegrini, G., Martini, L., Lenzi, M.A., Mao, L., 2020. An extraordinary event changed the (morphological) appearance of a famous Alpine stream. ISBN 0367627736. In: Proceedings of the 10th Conference on Fluvial Hydraulics (Delft, Netherlands, 7-10 July 2020). Taylor and Francis, pp. 1653–1658.
Piton, G., Recking, A., 2017. The concept of travelling bedload and its consequences for bedload computation in mountain streams. Earth Surf. Proc. Land. 42, 1505–1519.
Pomeroy, J.W., Xing, F., Marks, D., 2016. The Cold Rain-on-Snow Event of June 2013 in the Canadian Rockies - Characteristics and Diagnosis. Hydrol. Process. 30 (17), 2899–2914.
Rainato, R., Mao, L., García-Rama, A., Picco, L., Cesca, M., Vianello, A., Preciso, E., Scussel, G.R., Lenzi, M.A., 2017. Three decades of monitoring in the Rio Cordon instrumented basin: Sediment budget and temporal trend of sediment yield. Geomorphology 291, 45–56.
Rainato, R., Mao, L., Picco, L., 2018a. Near-bankfull floods in an Alpine stream: effects on the sediment mobility and bedload magnitude. Int. J. Sedim. Res. 33 (1), 27–34.
Rainato, R., Picco, L., Cavalli, M., Mao, L., Neverman, A.J., Tarolli, P., 2018b. Coupling climate conditions, sediment sources and sediment transport in an alpine basin. Land Degrad. Dev. 29 (4), 1154–1166.
Rainato, R., Mao, L., Picco, L., 2020. The effects of low-magnitude flow conditions on bedload mobility in a steep mountain stream. Geomorphology 367, 107345.
Recking, A., 2012. Influence of sediment supply on mountain streams bedload transport. Geomorphology 175–176, 139–150.
Reid, D.E., Hickin, E.J., 2008. Flow resistance in steep mountain streams. Earth Surf. Proc. Land. 33, 2211–2240.
Rickenmann, D., 1997. Sediment transport in Swiss torrents. Earth Surf. Proc. Land. 22 (10), 937–951.
Rickenmann, D., 2020. Effect of sediment supply on cyclic fluctuations of the disequilibrium ratio and threshold transport discharge, inferred from bedload transport measurements over 27 years at the Swiss Erlenbach stream. Water Resour. Res. 56 (11) e2020WR027741.
Rico, M., Benito, G., Barnolas, A., 2001. Combined palaeoflood and rainfall–runoff assessment of mountain floods (Spanish Pyrenees). J. Hydrol. 245, 59–72.
Rinaldi, M., Surian, N., Comiti, F., Bussettini, M., 2013. A method for the assessment and analysis of the hydromorphological condition of Italian streams: the Morphological Quality Index (MQI). Geomorphology 180–181, 96–108.
Ruiz-Villanueva, V., Badoux, A., Rickenmann, D., Böckli, M., Schläfli, S., Steeb, N., Stoffel, M., Rickli, C., 2018. Impacts of a large flood along a mountain river basin: the importance of channel widening and estimating the large wood budget in the upper Emme River (Switzerland). Earth Surf. Dyn. 6, 1115–1137.
Schoklitsch, A., 1962. Handbuch des Wasserbaues, third ed. Springer, Wien.
Scorpio, V., Crema, S., Marra, F., Righini, M., Ciccarese, G., Borga, M., Cavalli, M., Corsini, A., Marchi, L., Surian, N., Comiti, F., 2018. Basin-scale analysis of the geomorphic effectiveness of flash floods: A study in the northern Apennines (Italy). Sci. Total Environ. 640–641, 337–351. https://doi.org/10.1016/j.scitotenv.2018.05.252.
Shakti, P.C., Nakatani, T., Misumi, R., 2017. Hydrological simulation of small river basins in northern Kyushu, Japan, during the extreme rainfall event of July 5–6. J. Disaster Res. 13 (2), 396–409.
Stoffel, M., Bollschweiler, M., 2008. Tree-ring analysis in natural hazards research – an overview. Nat. Hazards Earth Syst. Sci. 8, 187–202.
Sholtes, J.S., Yochum, S.E., Scott, J.A., Bledsoe, B.P., 2018. Longitudinal variability of geomorphic response to floods. Earth Surf. Proc. Land. 43, 3099–3113.
Taylor, J., 1997. An Introduction to Error Analysis: the Study of Uncertainties in Physical Measurements, second ed. University Science Books, Sausalito, CA.
Turowski, J.M., Yager, E.M., Badoux, A., Rickenmann, D., Molnar, P., 2009. The impact of exceptional events on erosion, bedload transport and channel stability in a step pool channel. Earth Surf. Proc. Land. 34, 1661–1673.
Uchida, T., Sakurai, W., Iuchi, T., Izumiyama, H., Borgatti, L., Marcato, G., Pasuto, A., 2018. Effects of episodic sediment supply on bedload transport rate in mountain rivers. Detecting debris flow activity using continuous monitoring. Geomorphology 306, 198–209.
Vericat, D., Smith, M.W., Brasington, J., 2014. Patterns of topographic change in sub-humid badlands determined by high resolution multi-temporal topographic surveys. Catena 120, 164–176. https://doi.org/10.1016/j.catena.2014.04.012.
Vericat, D., Wheaton, J.M., Brasington, J., 2017. Revisiting the morphological approach: opportunities and challenges with repeat high-resolution topography. In: Tsutsumi, D., Laronne, J.B. (Eds.), Gravel-bed Rivers: Processes and Disasters, first ed. John Wiley & Sons Ltd, pp. 121–158.
Victoriano, A., Díez-Herrero, A., Génova, M., Guinau, M., Furdada, G., Khazaradze, G., Calvet, J., 2018. Four-topic correlation between flood dendrogeomorphological evidence and hydraulic parameters (the Portainé stream, Iberian Peninsula). Catena 162, 216–229.
Wheaton, J.M., Brasington, J., Darby, S.E., Sear, D.A., 2010. Accounting for uncertainty in DEMs from repeat topographic surveys: Improved sediment budgets. Earth Surf. Proc. Land. 35 (2), 136–156. https://doi.org/10.1002/esp.1886.
Wheaton, J.M., Brasington, J., Darby, S.E., Kasprak, A., Sear, D., Vericat, D., 2013. Morphodynamic signatures of braiding mechanisms as expressed through change in sediment storage in a gravel-bed river. J. Geophys. Res. Earth Surf. 118 (2), 759–779. https://doi.org/10.1002/jgrf.20060.
Wicherski, W., Dethier, D.P., Ouimet, W.B., 2017. Erosion and channel changes due to extreme flooding in the Fourmile Creek catchment, Colorado. Geomorphology 294, 87–98.
Wyzga, B., Radecki-Pawlik, A., Galia, T., Plesiński, K., Škarpich, V., Dušek, R., 2020. Use of high-water marks and effective discharge calculation to optimize the height of bank revetments in an incised river channel. Geomorphology 356, 107098.
Yochum, S.E., Sholtes, J.S., Scott, J.A., Bledsoe, B.P., 2017. Stream power and geomorphic change during the 2013 Colorado front range flood. Geomorphology 292, 178–192.
Zink, J.M., Jennings, G.D., 2014. Channel roughness in North Carolina Mountain Streams. J. Am. Water Resour. Assoc. (JAWRA) 50 (5), 1354–1358.